A MODELLING STUDY ON THE LATERAL LOAD CAPACITY OF STEEL-FIBER CONCRETE PILES

A Thesis Submitted to the
Graduate School of Natural and Applied Sciences of
Dokuz Eylül University
In Partial Fulfillment of the Requirements for
the Degree of Master of Science in Civil Engineering, Geotechnics Program

by

Cihan Taylan AKDAĞ

July, 2004
İZMİR

150954

M.Sc. THESIS EXAMINATION RESULT FORM

We certify that we have read this thesis and **"A MODELLING STUDY ON THE LATERAL LOAD CAPACITY OF STEEL-FIBER CONCRETE PILES"** completed by **CİHAN TAYLAN AKDAĞ** under supervision of **Assist. Prof. Dr. GÜRKAN ÖZDEN** and that in our opinion it is fully adequate, in scope and in quality, as a thesis for the degree of Master of Science.

Assist. Prof. Dr. Gürkan ÖZDEN

Supervisor

Prof. Dr. Arif S. KAYALAR

(Committee Member)

Prof. Dr. Necdet Türk

(Committee Member)

Approved by the

Graduate School of Natural and Applied Sciences

Prof.Dr.Cahit Helvacı

Director

ACKNOWLEDGMENTS

The author hopes that this study will contribute to the geotechnical engineering proficiency. Besides, he believes that the process has been instructive that the acquired knowledge required patience, delicate work, teamwork, and hard working.

The author wishes to express his gratitude to his supervisor, Assist. Prof. Dr. Gürkan ÖZDEN, for his guidance and invaluable suggestions at all phases of this study.

He sincerely would like to thank to his friends, Serkan MISIR for his support, Vedat KUŞKU, and Metin TÜLÜ for their helps at the laboratory work. Nevertheless he would like to thank to Mehmet YERLİKAYA for his contribution such as providing fibers and sharing his document archive. The support of ZETAS and GEOTEST must also be mentioned here since this study would face tremendous difficulties without material support of these geotechnical companies.

Finally, he also thanks his family for their material and spiritual support and of course for their endless sensitivity and patience to his all matters since the beginning.

Cihan Taylan AKDAĞ

ABSTRACT

The need for more ductile piles has been strongly felt in recent years as the damaged pile documents increased following major earthquakes of Kobe, Loma Prieta and Marmara. The objective of this study was to investigate static lateral load behavior of SFRC piles and compare their test performance with that of the conventional concrete pile.

A model pile study to investigate lateral load capacity of steel fiber concrete (SFRC) piles has been planned, and an appropriate testing system was constituted. According to mix design study, totally ten piles for five concrete types were prepared for testing. Tests were performed using four model piles each belonging to a different pile type; Concrete, by the volumetric fiber content of 1.5% (ZP305), 1.0% (ZP305), and 0.75% (ZP305) + 0.25% (micro fiber). Remained piles were spared for subsequent research studies due to time limitations.

Test results such as moment distribution along the pile, and pile head deformation has been evaluated, and discussed by the soil-structure interaction approach. It was observed that addition of steel fibers improve the ductility of piles significantly. It was considered that the projected model tests would constitute a firm ground for future in-situ field pile loading tests of SFRC piles.

Keywords: Concrete piles; Steel fiber reinforced concrete; Lateral load; Modeling

ÖZET

Hasar görmüş kazıklarla ilgili kayıtların, Kobe, Loma Pritea ve Marmara gibi önemli depremlerle artışı, dayanımı daha yüksek kazık ihtiyacını son yıllarda daha da güçlü bir şekilde hissettirmektedir.Bu çalışmanın amacı, çelik lifli beton kazıkların yatay yük altındaki davranışını araştırmak ve çelik lifli beton kazıklarla beton kazıkları deney performansı açısından karşılaştırmaktır.

Lifli beton kazıkların yatay yük altındaki kapasitelerinin, model kazık çalışması ile araştırılması planlanmış olup, uygun bir deney sistemi oluşturulmuştur. Hazırlanmış olan beton karışım dizaynı baz alınarak, 5 tipte olmak üzere, toplam 10 adet model kazık üretilmiştir. Hacimce oranı ve lif tipi; 1.5% (ZP305), 1.0% (ZP305),0.75% (ZP305) + 0.25% (micro fiber) olan çelik lifli üç adet ve beton olarak bir adet, farklı tiplerde dört adet model kazık deneyi gerçekleştirilmiştir.Geriye kalan kazıklar zaman sınırı nedeniyle ileriki çalışmalarda kullanılmak üzere ayrılmıştır

Kazık boyunca moment dağılımı ve kazık başı deformasyonları olarak elde edilen deney sonuçları, yapı zemin etkileşimi yaklaşımıyla değerlendirilmiştir.Bu çalışmada çelik lif kullanımının, kazığın mukavemet özelliklerini önemli bir şekilde etkilediği gözlemlenmiştir.Tasarlanmış olan model çalışmasının, arazide yapılacak olan çelik lifli beton kazık yükleme deneylerine sağlam bir temel oluşturacağı düşünülmektedir.

Anahtar sözcükler: Beton kazıklar; Çelik lifli beton; Yatay yük; Model

CONTENTS

Chapter Four

MODELING

Chapter Five

CONCRETE MIX DESIGN

Chapter Six

RESULTS and DISCUSSION

Chapter Seven

RESULTS and DISCUSSION

LIST OF TABLES

Page

LIST OF FIGURES

Page

CHAPTER ONE
INTRODUCTION

Although pile foundations are primarily designed to overcome foundation settlement problem, it is quite common to see that lateral loads govern pile foundation design especially in seismically active areas. This fact, however, is reflected either in pile section dimensions or amount of reinforcement needed in reinforced concrete piles.

Pile foundations are more expensive than shallow foundations because of their construction technology. Because of this reason possibly, people believe that piles cannot be damaged during earthquakes. However, there is evidence that piles may be damaged under seismic loads (Mizuno, 1987). Examples to pile damage are given in Figures 1.1a and 1.1b.

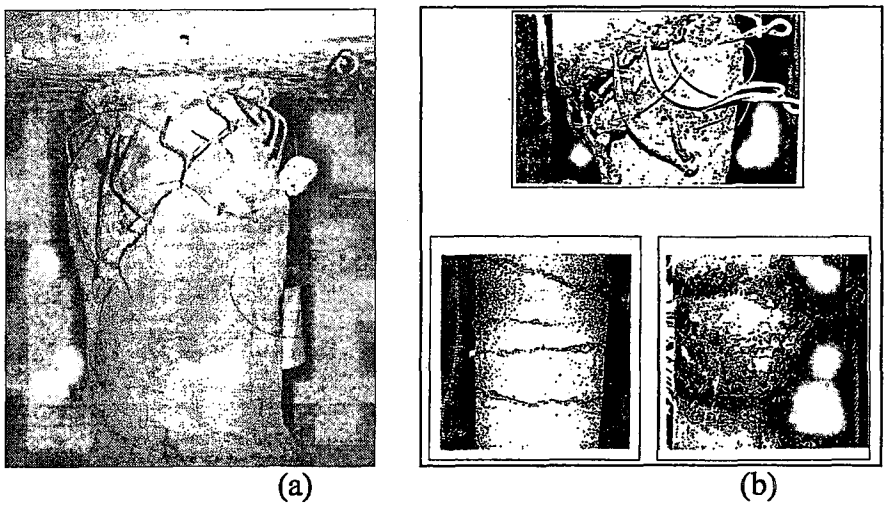

Figure 1.1 Examples to damaged piles during earthquakes (a) Due to inertial loading, (b) Due to inertial loading *(top)*, due to kinematical loading *(lower two)* (Ozden, G., 1999)

The need for more ductile piles has been strongly felt in recent years as the damaged pile documents increased following major earthquakes of Kobe, Loma Prieta and Marmara. For instance it was stated that pile research should be towards the development of ductile piles in order to understand influence of inelastic pile behavior on structural response (Gazetas & Mylonakis, 1998).

Based on above considerations a model pile study to investigate lateral load capacity of steel fiber concrete (SFRC) piles has been planned since steel fibers have been in use to produce ductile structural elements for many years. The goal was to study SFRC pile behavior in dry cohesionless soils and to gain insight for the mechanisms actively participating in SFRC pile-soil interaction.

CHAPTER TWO
SCOPE

This study presents experimental research to investigate the effects of steel fiber addition to the behavior of laterally loaded piles. The essential concept is to constitute a model testing system to observe the soil–pile interaction under static lateral load successfully.

The literature research study has been done about laterally loaded piles, steel fiber reinforced concrete (SFRC) and pile model studies. There is a bulk of research study regarding in-situ tests, and laboratory-modeling studies on laterally loaded piles under static and cyclic loading conditions.

Although there are several studies on steel fiber reinforced concrete in the literature as explained in Chapter Three, there are almost no significant studies about model pile studies made of SFRC material. Consequently, some concepts have been developed for such a modeling work, and details are given in Chapter Four.

The starting point of laboratory work has been to establish fundamental parameters of the mix design of conventional concrete and SFRC. Trial batches were cast in order to verify target properties. Then final batch design was established, and the mechanical properties of resultant conventional and SFRC concrete specimens were obtained as described in Chapter Five.

A total of ten piles out of five model types were prepared for testing. One additional model pile has been produced for calibration studies. Two model piles for each type were cast. Model piles were equipped using special concrete type strain-

gages in order to capture elastic curve under lateral loading. For calibration purposes moment generation technique was used to develop a relationship between measured voltage and bending moment. A reinforced concrete model pile was used for this purpose. Two piles were placed into the testing pool for each test. Then transducers placed on the top of the pile to determine the pile head deformation. Strain gages and displacement transducers were all conditioned and digitally converted using Wheatstone bridges and a data acquisition device, respectively. These aspects of this study are also given in the fourth chapter.

Tests were performed using four model piles each belonging to a different pile type. Remained piles were spared for subsequent research studies. The results have been evaluated and discussed in the sixth chapter. The seventh chapter has concluded the study where significant findings and suggestions for future studies are included.

CHAPTER THREE
A REVIEW OF STEEL FIBER REINFORCED CONCRETE

3. Steel Fibers

Fibers have been in use to reinforce brittle materials. In ancient times, straw was used to reinforce sun-baked bricks, and horsehair was used to reinforce plaster. In modern times, however, fibers have been utilized in a wide range of engineering materials (including ceramics, plastics, cement, and gypsum products) to enhance engineering characteristics. Such characteristics include tensile strength, compressive strength, elastic modulus, crack resistance, crack control, durability, fatigue life, resistance to impact and abrasion, shrinkage, expansion, thermal characteristics, and fire resistance (ACI, 1996).

Experimental trials involving the use of discontinuous steel reinforcing elements to improve the properties of the concrete date from 1910. It was stated in the above-mentioned source that during the early 1960s the first major investigation was made to evaluate the potential of steel fibers as reinforcement for concrete (Romualdi and Batson, 1963). A substantial amount of research, development, experimentation, and industrial application of steel fiber reinforced concrete has occurred since then. Naaman (2003) notes that cementitious matrices such as concrete have low tensile strength and fail in a brittle manner. Adding short needle-like fibers to such matrices enhances their mechanical properties, particularly their toughness, ductility and energy absorbing capacity under impact. The addition of steel-fibers significantly improves many of the engineering properties of mortar and concrete, notably impact

strength and toughness. Flexural strength, fatigue strength, tensile strength and the ability to resist cracking are also enhanced (Nataraja et al., 1999).

Steel fiber reinforced concrete (SFRC) is a cement-based material reinforced with discontinuous discrete steel fibers. When steel fibers are added to a concrete mixture, they are randomly distributed and act as crack arrestors. Pulling out of fibers require more energy, giving a substantial increase in toughness. In tension, SFRC fails only after the steel fiber breaks or is pulled out of the cement matrix.

SFRC is a composite material whose properties can be closely related to the properties of fiber (volume percentage, strength, elastic modulus and a fiber bonding parameter of the fibers), concrete properties (strength, volume percentage, and elastic modulus), and the properties of the interface between the fiber and the matrix.

Use of SFRC has steadily increased during the last 25 years. It has advantages over conventional reinforced concrete for several end uses in construction. Considerable developments have taken place in the field of steel-fiber reinforced concrete as reported by Bentur and Mindess (1990). The current field of application of steel-fiber reinforced concrete includes highway and airfield pavements, hydraulic structures, shotcrete for tunnel lining, rock slope stabilization, lagging for the support of excavation, pile foundations and structural element connections.

3.1 Classification of Discontinuous Fibers

Short fibers used in concrete can be characterized in three different ways. Firstly classification can be made according to the fiber material; natural organic (such as cellulose, sisal, jute, bamboo, etc.); natural mineral (such as asbestos, rock-wool, etc.), and man-made material (such as steel, titanium, glass, carbon, polymers or synthetic, etc). Secondly, they can be classified according to their physical/chemical properties such as density, surface roughness chemical stability, non-reactivity with the cement matrix, fire resistance or flammability, etc. Finally, their mechanical properties such as tensile strength, elastic modulus, stiffness, ductility, elongation to

failure, surface adhesion property, etc can play an important role in the classification. Moreover, once a fiber has been selected, an infinite combination of geometric properties related to its cross sectional shape, length, diameter, and surface deformation can be selected to define its general characteristic. The cross section of the fiber can be circular, rectangular, diamond, square, triangular, flat, polygonal, or any substantially polygonal shape. Thus fibers can be smooth, indented, deformed, crimped, coiled, and twisted, with end hooks, paddles, buttons, or other anchorage.

3.2 Geometrical and Physical Properties of Fiber

Most common steel fibers are circular in cross-section, with a diameter ranging from 0.4 to 0.8 mm, and a length in a range of 25~60 mm. Their aspect ratio, that is, the ratio of length to diameter or equivalent diameter, is generally less than 100, with a common range of 40 to 60, which is sufficiently small for the fibers to be randomly dispersed in an unhardened concrete mixture following usual mixing procedures.

Steel fibers have a relatively high strength and modulus of elasticity. They are protected from corrosion by the alkaline environment of the cementitious matrix, and their bond to the matrix can be enhanced by mechanical anchorage or surface roughness. Long-term loading does not adversely influence the mechanical properties of steel fibers.

3.3 Fiber Content and Volume Fraction of Fibers

Due to the formulation of the mechanics of the composite, the fiber content in cement matrices is specified by volume fraction of the total composite. The fiber volume content, V_f (%) in typical fiber reinforced concrete applications is shown in Table 3.1.

Table 3.1 Typical fiber volume fractions in concrete applications (Naaman,2003)

Material	Range of V_f	Remark
FRC-Fiber reinforced concrete	$V_f \leq 2\%$	Fibers are premixed with the concrete matrix. Finer aggregates may be needed.
HPFRCC-High Performance Fiber Reinforced Cement Composites.	$V_f \geq 1\%$ or $V_f \geq (V_f)_{crictical}$	Strain hardening and multiple cracking characteristics in tension. With proper design, critical V_f can be less than 2%.
Shotcrete (steel fibers)	$V_f \leq 3\%$	Applications in tunnel lining and repair.
Spray Technique (glass fibers)	$4\% \leq V_f \leq 7\%$	Applications in cladding and panels.
SIMCON (steel fibers)	$4\% \leq V_f \leq 6\%$	Slurry Infiltrated Mat Concrete. A prefabricated fiber mat is needed.
SIMCON (PVA fibers)	$V_f \approx 1\%$	Recently available
SIFCON (steel fibers)	$4\% \leq V_f \leq 15\%$	Slurry Infiltrated Fiber Concrete, Fibers are replaced in a mold and infiltrated by a fine cementitious slurry matrix.

3.4 Fiber-Matrix Reinforcing Effectiveness

Both analysis and experimental test results suggest that, in order to be effective in concrete matrices, fibers must have the following properties (Naaman, 2003):

1) Tensile strength should be significantly higher than that of the concrete (at least two or three orders of magnitude);
2) Bond strength with the concrete matrix should be preferably of the same order as or higher than the tensile strength of the matrix; and
3) Elastic modulus in tension should be significantly higher than that of the concrete matrix. The Poisson's ratio and the coefficient of thermal expansion should preferably be of the same order for both the fiber and the matrix.

3.5 Influence of Steel Fibers on the Properties of Concrete

Steel fibers improve the ductility of concrete under all modes of loading. The degree of improvement, however, varies in compression, tension, shear, torsion, and flexural loading modes. Especially in recent years a substantial amount of research, development, testing, and application of steel fiber reinforced concrete has been encountered in the literature.

The results obtained with the uniaxial compression tests with fiber reinforced concrete have revealed a slight increase in the compression strength, stiffness, and strain at peak load and a substantial increase in the post peak energy absorption capacity (Fanella & Naaman, 1985; Ezeldin & Balaguru, 1992). In compression, the ultimate strength is only slightly affected by the presence of fibers with appropriate utilization of the fibers with a volume fraction of approximately 1.5%. Observed increases range between 0 and 15% (ACI 544.1R-96).

In recent years, the demand for high strength concrete has been growing at an ever-increasing rate, and many new structures have been built using concrete with a compressive strength as high as 100 MPa. Recent studies have, however, shown increasing evidence that the brittle nature of high strength concrete can be overcome by addition of discrete fibers of short length and small diameter in the concrete mix. Adding fibers improve some mechanical properties of high-strength concrete such as tensile strength, compressive strength and flexural energy absorption capability (Mansur et al., 1999; Rossi, 2000; Eren & Celik, 1997; Banthia et al., 2000; Krumbach et al., 1998). A case history for the application of high-strength fiber reinforced concrete includes a repair project of a parking garage in Vancouver (Banthia et al., 2000). Another application of steel fibers in high-strength concrete is the construction of two highway bridges on the Bourg lés Valence bypass in Drome Region of France (Simon et al., 2002).

The ductile behavior of reinforced concrete structures dominantly depends on the reinforcement detailing of the beam-column joints. A recent study on this subject indicates that using SFRC could increase the ductility and strength capacity reducing the cost of steel reinforcement in the critical regions (Gençoğlu & Eren, 2002).

With the increasing number of applications in practice, the demand for standard testing methods and design rules for SFRC arises. A procedure to develop a reliable, bilinear stress-crack width relationship to describe the post-cracking behavior of SFRC by inverse analysis has been proposed (Kooiman et al., 2000). Kützing and König developed a theoretical model to calculate the deformation capacity and

fracture mechanical values of SFRC. According to this study ultimate shear load, fracture behavior of elements under compression can be estimated (Kützig & König, 1999).

The primary advantage in using SFRC is its high flexural performance. The most significant improvement by adding fibers to concrete is the substantial increase in the energy absorption capacity (Choi & Lee, 2002; Barros & Figueiras, 1999; Mailhot et al., 2000; Dry & Corsaw, 2003). Steel fibers increase the deformation capacity of concrete. In most cases, steel fibers are pulled out as a result of debonding rather than being ruptured under tensile stress. If the element is loaded following the formation of the concrete matrix, the stress is adsorbed as a result of the bridging fibers and the bending moments are redistributed. The concrete element does not fail spontaneously when the matrix is cracked. Steel fibers enhance the energy absorption and the ductility of the concrete under tensile stress not only for post-crack, but also before the peak load. The studies demonstrate that the flexural strength of SFRC is about 50 to 70 percent more than that of the unreinforced concrete matrix in the traditional third-point bending test (Shah & Rangan, 1971; Johnston, 1974).

In present study the structural ductility and energy absorption capability of SFRC piles is compared with that of reference conventional concrete piles with the application of lateral static load. Under lateral loading conditions attention should be paid for the flexural strength and deflection capacity of piles are the main mechanical characteristics. Although considerable work has been done on the flexural strength and stress-strain characteristics of SFRC, few studies and applications were done for the efficiency of steel fibers as reinforcement in conventional concrete piles. In a recent study test data are provided on the seismic behavior of SFRC piles (Bodin & Madhkhan, 2002). Four large-scale specimens are subjected to a combination of constant axial load and alternating cyclic flexure. Piles, however, were not embedded in the soil. Instead bending test with mid span loading method was used on the model piles with a diameter of 0.50 m and a length of 3 m. According to this study, axially loaded SFRC piles exhibit higher ductility and a better energy dissipation capacity than those of the reinforced concrete. But without axial load the strength of SFRC is decreasing similar to the behavior of conventional reinforced concrete columns. In the above-mentioned study, Bodin and Madhkhan emphasize that the decrease in the

flexural strength of the SFRC piles without axial load is on the order of 300% to 400% and is significantly higher than that of the RC piles in similar loading condition.

A well documented use of SFRC piles has taken place in the construction of flood protection wall for the lower access road leading to the power generation house of Horse Mesa Dam located in 100 km northeast of Phoenix Arizona (Bayasi & Downey, 1995). It was determined that the sides of the access road would be incapable of withstanding a large discharge. It should be mentioned that the road has been washed out six times since February 1968. Pile wall construction was proposed to prevent the road. The engineers decided to construct composite piles consisting of wide flange steel section encased within steel fiber reinforced grout. After the boring was made steel member was placed in the hole. Then steel fiber reinforced grout was placed into the casing. Pile manufacturing procedure followed in this project is also shown in Figure 3.1. According to Bayasi & Downey using steel fiber reinforced concrete has perhaps made this project possible. They noted as "Steel fibers confine plain concrete and enhance its integrity and crack resistance. With steel fiber grout encasing the W sections in the composite piles of the Dam adequate protection was achieved". Bayasi & Downey noted that conventional grout was deemed inadequate especially under impact loads from water carried debris. Steel fiber reinforced grout was needed for adequate lateral support. Comparison of stress-strain behavior of the SFRC mix design as used in the Mesa Dam project piles with those of traditional concrete mix is shown in Figure 3.2.

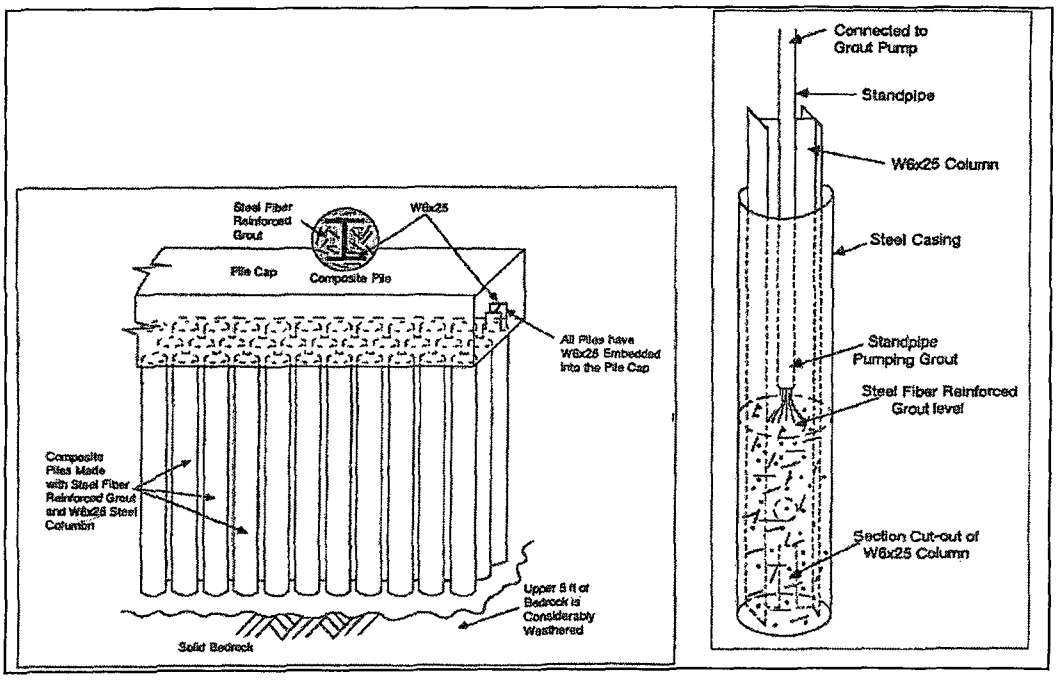

Figure 3.1 Piling arrangement and manufacturing procedure in Mesa Dam project (Bayasi & Downey, 1995)

The stress-strain curves shown in the figure were produced in the flexural load-deflection four-point loading test according to ASTM C 1018. As one can note in Figure 3.2 that overall ductility of the SFRC mix is superior to traditional concrete indicate higher energy absorption capacity. The peak strength is also higher for SFRC mix being 13.2% larger than that of traditional concrete.

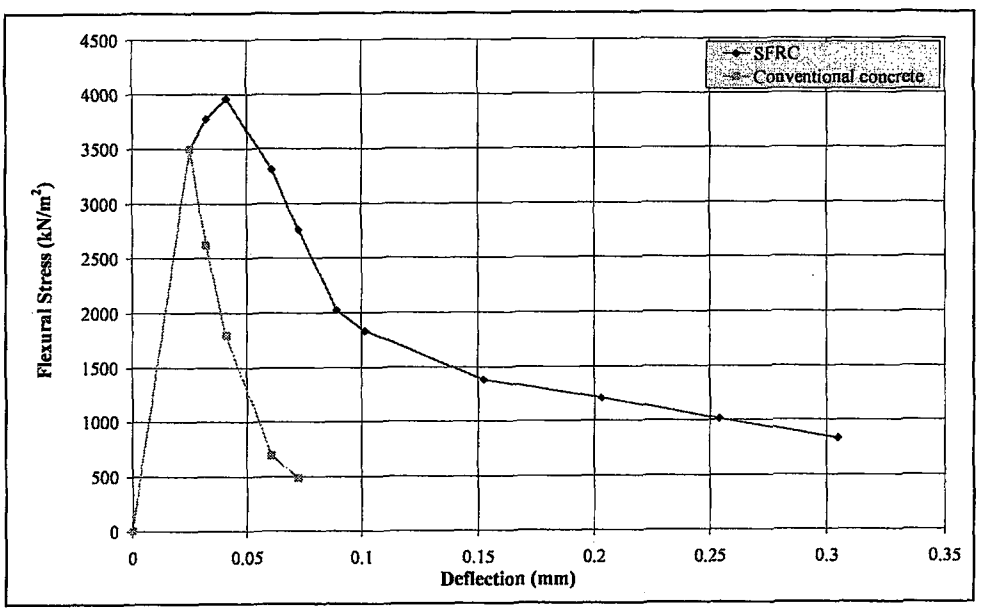

Figure 3.2 Comparison of flexural behavior of SFRC and conventional concrete

CHAPTER FOUR
MODELING

4.1 Testing System

The objective of this study was to investigate static lateral load behavior of SFRC piles and compare test performance with that of the conventional concrete pile. Therefore, it has been necessary to establish a small-scale testing system. It was considered that the projected model tests would constitute a firm ground for future in-situ field pile loading tests of SFRC piles. The overall testing system has been modeled to consist of the following basic items.

a. Testing pool
b. Testing frame
c. Test pile
d. Loading mechanism (loading reel, steel rope and metal load transfer ring)

The system also involves measurement units located along the pile (i.e. strain gages) and at the pile head (i.e. displacement transducer). Strain gages were bonded on the pile at equal spacing using appropriate adhesives to obtain bending moment of the pile during lateral loading. Three displacement transducers were located at the pile top to measure pile head displacement. Strain gages and displacement transducers were all conditioned and digitally converted using Wheatstone bridges and a data acquisition device, respectively.

Strain-gages located on the pile are shown in Figure 4.1. Pile-head transducers are shown in Figure 4.2. General view of the overall testing system is given Figure 4.3.

The cross-section of the concrete pool, model pile and loading mechanism is illustrated in Figure 4.4. Details of the testing system are given in subsequent sections of this chapter.

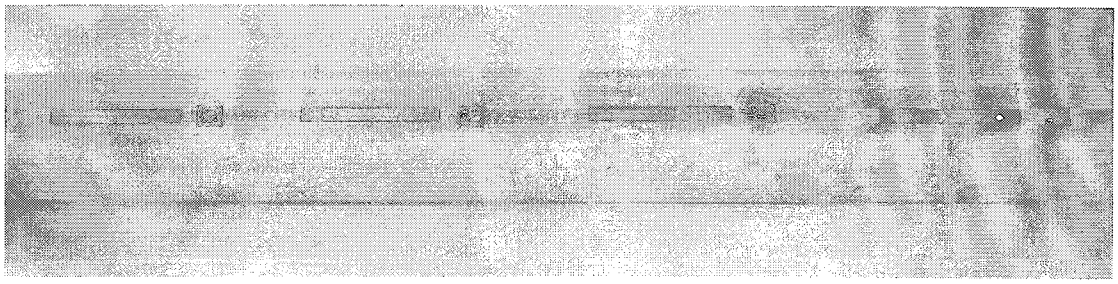

Figure 4.1 Strain-gages bonded on the model pile

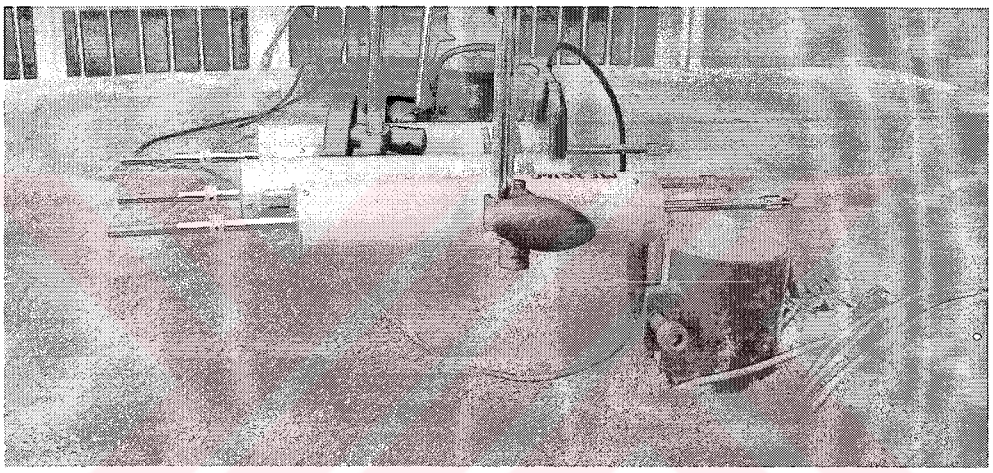

Figure 4.2 Model pile-head displacement transducers

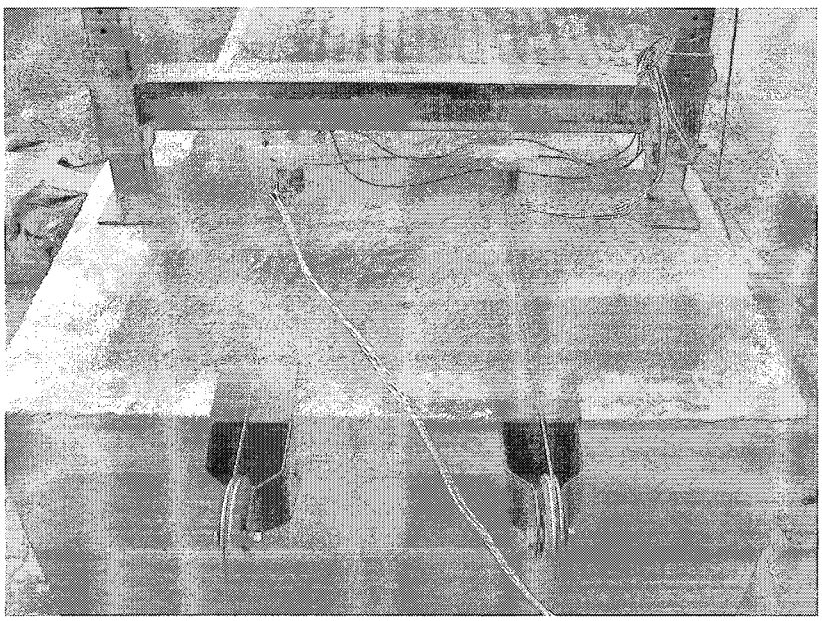

Figure 4.3 General view of the testing system

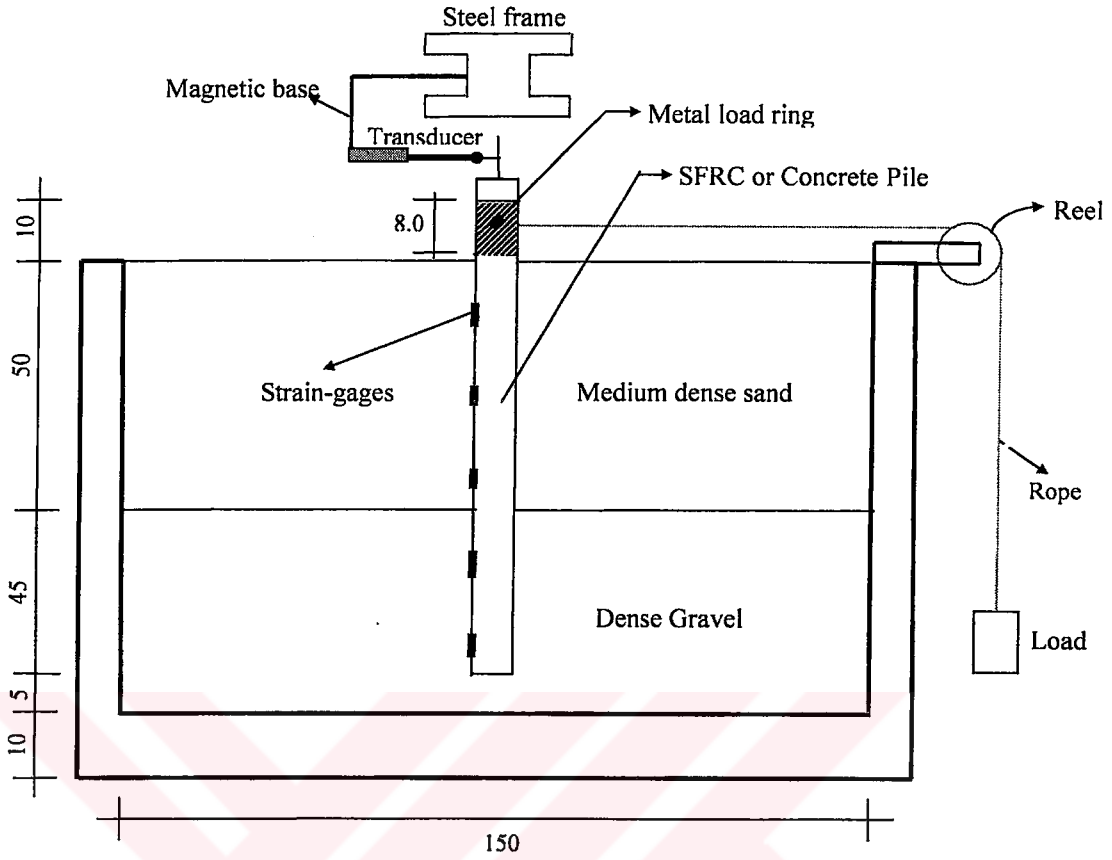

Figure 4.4 Cross-sectional view of the testing system

4.2 Model Pile

4.2.1. Pile Dimensions

The steel fibers, SFRC mix standards and the concrete model testing pool already available prior to this study governed dimensions of the model pile. These factors were all taken into consideration to determine optimum dimensions for the model pile.

Hooked-end straight steel fiber ZP30/0.5 with an aspect ratio L/d=60 was used L and d being the length (30mm) and width (0.5mm) of the fiber, respectively. The manufacturer reported the specific gravity of the fiber as 7.8 kg/dm^3. This type of steel fiber is the smallest hooked-end fiber to be used in the mix and readily available in the Turkish market. Besides short fibers with an aspect ratio less than 50 are reported to be not able to interlock and can easily be dispersed by vibration (ACI,

96). The steel fiber dictated the maximum size of the aggregate in the mix since fiber length should be at least 1.5 to 2 times the diameter of the maximum aggregate (DSİ, 1999). The maximum aggregate size has been decided as 12.5 mm to comply with this requirement (l_{fiber}=30>2x12.5=25mm).

Another factor that would affect the maximum aggregate size in the mix has been considered as the size of the element since too small molds with respect to the maximum aggregate would result in the formation of gaps and honeycomb voids at the surface of the element. A general criterion in order to avoid such disturbances has been stated, as the maximum size of aggregate particles generally should not exceed one-fifth the narrowest dimension of the concrete member or three-fourths the clear spacing between reinforcing bars (Kosmatka & Panarese, 1994).

Theoretical solutions and experimental results for a laterally loaded pile showed that induced stresses and deformations are rapidly damped with third power of the pile radius in the soil (Baguelin et al., 1977). The soil zone that is heavily affected by pile deformation has been reported as two-pile radius and loading influence becomes negligible beyond eight-pile radius. These considerations can be summarized as in Equations 4.1a and 4.1b:

$$\sigma_r, u_r \ \alpha \ \frac{1}{r^3} \qquad 4.1a$$

$$\sigma_r, u_r \ \approx \ 0 \ @ \ \ x \geq 8r \qquad 4.1b$$

where σ_r, u_r, r, and x are radial stress, radial deformation, pile radius and distance along loading direction, respectively.

Considering the above-explained criteria the diameter of the model pile has been decided as 7.0cm. The x≥8r lateral loading criterion is also complied with when the model pile is located at the center of the testing pool as illustrated in Figure 4.4. Selecting model pile diameter as 7.0 cm is also compatible with minimum element

diameter requirement of 5 times the maximum aggregate size in the mix (d_{pile}=70 > 5x12.5 = 62.5mm).

One should notice that 7.0 cm pile diameter seems to be appropriate for the selected steel fiber type since SFRC has long been used in concrete pavement and slab applications with a thickness as small as 10 cm. There were no clear suggestions for the selection of element size with respect to steel fiber dimensions in the literature. This aspect of model pile diameter selection, however, needs further study since damaged pile sections indicated some fiber segregations and lump formations.

The length of the model pile has been set as 1.05m in order to keep 0.45m of the length inside the dense gravel layer so that the pile would fail either it behaves as a flexible or rigid pile. The important point was to avoid the rigid motion of the pile in sand and gravel layers. This was deemed essential for SFRC and concrete piles since it was desired to continue lateral loading until failure. As shown in Figure 4.4 the length of the pile embedded in medium dense sand layer became 0.5m leaving 0.10m long portion above the sand for lateral load application and pile head dispiacement transducer deformation readings. The gap between the pile tip and testing pool therefore has been set as 0.1m.

4.2.2. Model Pile Instrumentation

Model piles were equipped using special concrete type strain-gages in order to capture elastic curve under lateral loading. These strain-gages were much longer than traditional ones in order to compensate small voids and thin cracks that usually exist on most concrete elements. Strain-gages are made by Kyowa with a model number of SKW-10552. Each gage is 60mm long with a gage resistance of 120.0±0.4Ω. Gage factor for these strain-gages is 2.09±1.0%. These gages were bonded to the model piles using PC-12.CC-35 type cement of the Kyowa Company. Before adhesive application the surface of the model pile has been sanded using a thin sandpaper to obtain a surface as smooth as possible. Then this surface was washed by means of regular grease and oil solving chemical such as acetone.

Signal carrying shielded cable 4m in length and gage wires were soldered to the soldering terminal correspondingly to provide a firm connection.

Once the gages were bonded to the pile using this adhesive with great care, they were shielded against moisture and accidental mechanical damages. A regular silicon layer was applied as shock absorber after the gage was completely covered by a special wax coating to keep off the moisture. No curing was necessary for adhesive and wax applications whereas almost one day was needed for the hardening of the silicon coating. The cross-sectional view of the covered gage is shown in Figure 4.5.

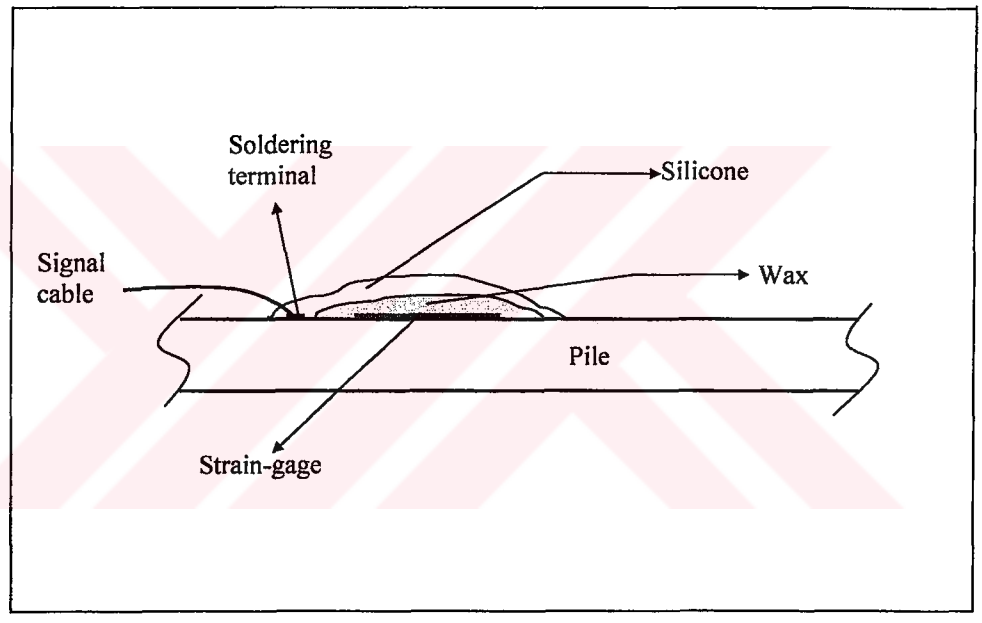

Figure 4.5 Typical strain-gage application

Five strain-gages were installed on each model pile. The distance between any two gage was kept equal and set to 18cm. The distances to the top and tip of the pile of the corresponding gages were 23cm and 10cm, respectively. The positions of the strain-gages scheme are also shown in Figure 4.6. Gages were tagged with ascending numbers from the tip of the pile to the top. Overall instrumentation was so arranged that the elastic curve of the pile during loading would be obtained in satisfactory accuracy.

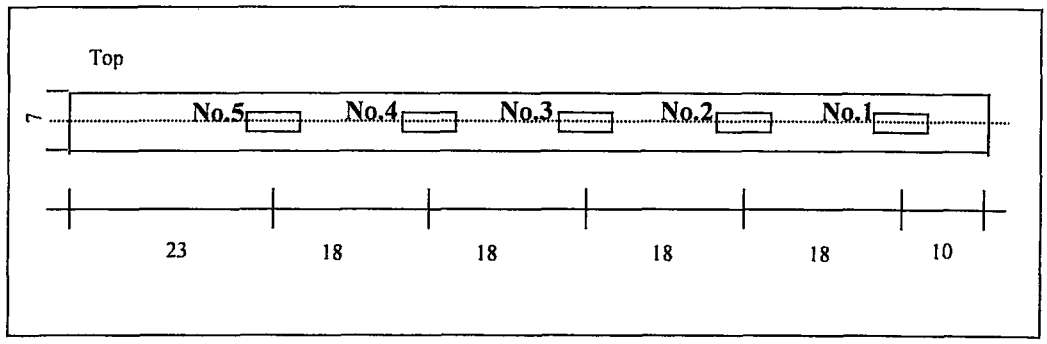

Figure 4.6 Strain-gage positions on the model pile

4.2.3. Placement of the Model Piles in Testing Pool

Since preparation of the test gravel and sand layers within the testing pool takes long time and demands significant man power, successive testing of two model piles in a single shift of soil profile was planned in order to provide economy for time and man power. However, it was necessary to check applicability of such testing style to demonstrate shadowing effect, if any, between the piles would be negligible. Checks were performed based on the formation of the passive wedge in front of the loaded pile:

$$BD = (H - x)\tan\beta \qquad 4.2a$$

$$\beta = 45 + \frac{\phi}{2} \qquad \alpha = \phi/2 \qquad 4.2b$$

$$CD = EF = BD \cdot \tan\alpha = (H - x) \cdot \tan\beta \cdot \tan\alpha \qquad 4.2c$$

$$DE = BG = 2r \qquad CF = 2CD + BG \qquad 4.2d$$

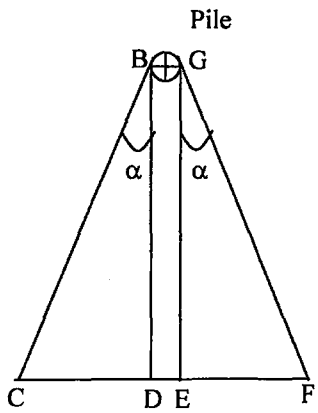

ϕ=34,5° (Explained later in this chapter)

H=0.95m (embedded pile length)

x=0.5 (distance from the pile top)

β= wedge angle

α= fanning angle

r=3.5cm (pile radius)

CF=60cm

BD=86cm

The above shown wedge dimensions in the plan can be used to demonstrate the possibility of interference between two piles as in Figure 4.7 if the piles are placed at the center of the pool along the longer axis:

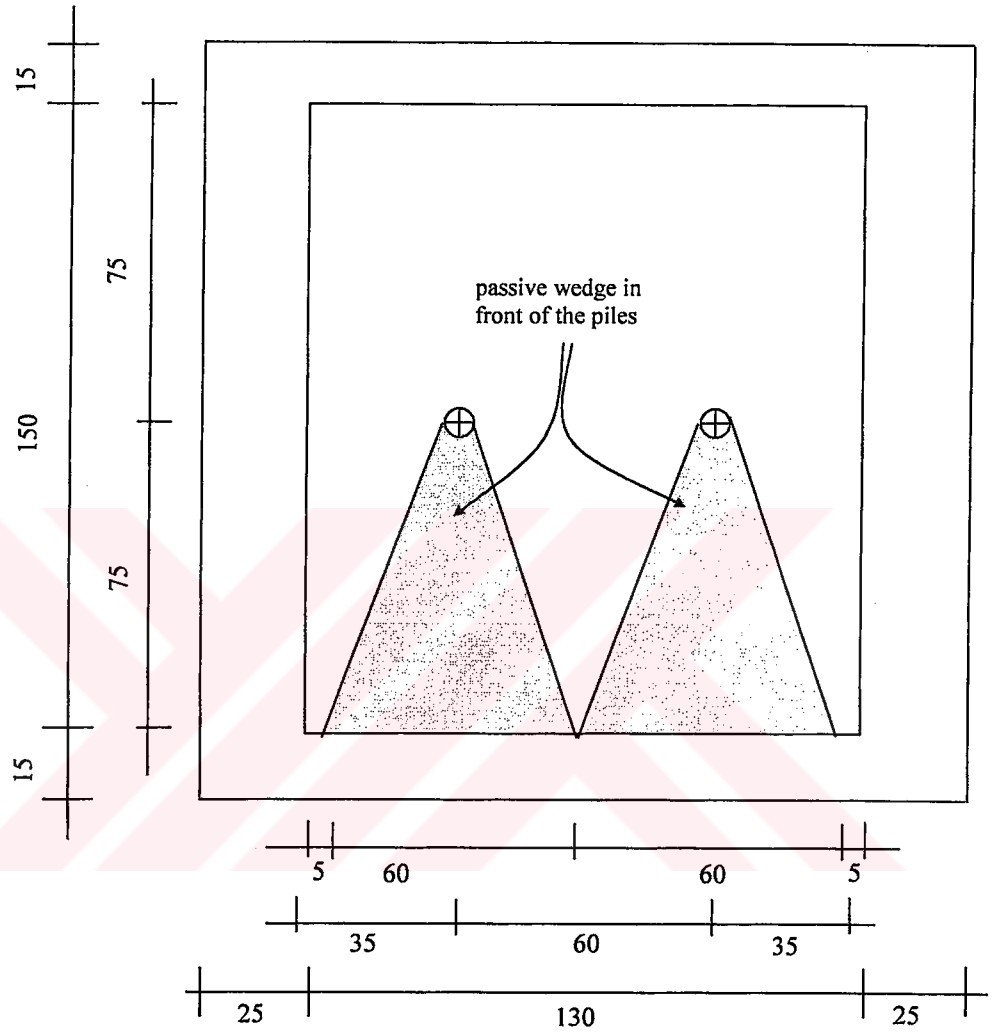

Figure 4.7 Placement of the piles and expected passive wedge formation

As one can notice in Figure 4.7 no significant interference between the wedges of the two piles are expected. Besides, it should be kept in mind that the piles would be loaded separately.

Placement of the gravel and sand layers had to follow a certain order. Firstly, the gravel layer has been placed by compacting it using a steel rod 8mm in diameter, and then two holes were formed until 5cm distance is left to the bottom of the pool.

Following this the piles were founded in the gravel layer. The gravel surrounding the piles was re-compacted after the piles were placed. After this application sand was placed above the gravel at 5cm thick layers each compacted by dropping a constant weight to obtain medium dense sand condition. Both sand and gravel layers were compacted in dry condition. The geotechnical characteristics of sand and gravel layers are given in the following subsection. The above described preparation and placement of soil and piles are also shown by Figures 4.8 and 4.9.

Figure 4.8 Placement of the piles and soil layer preparation

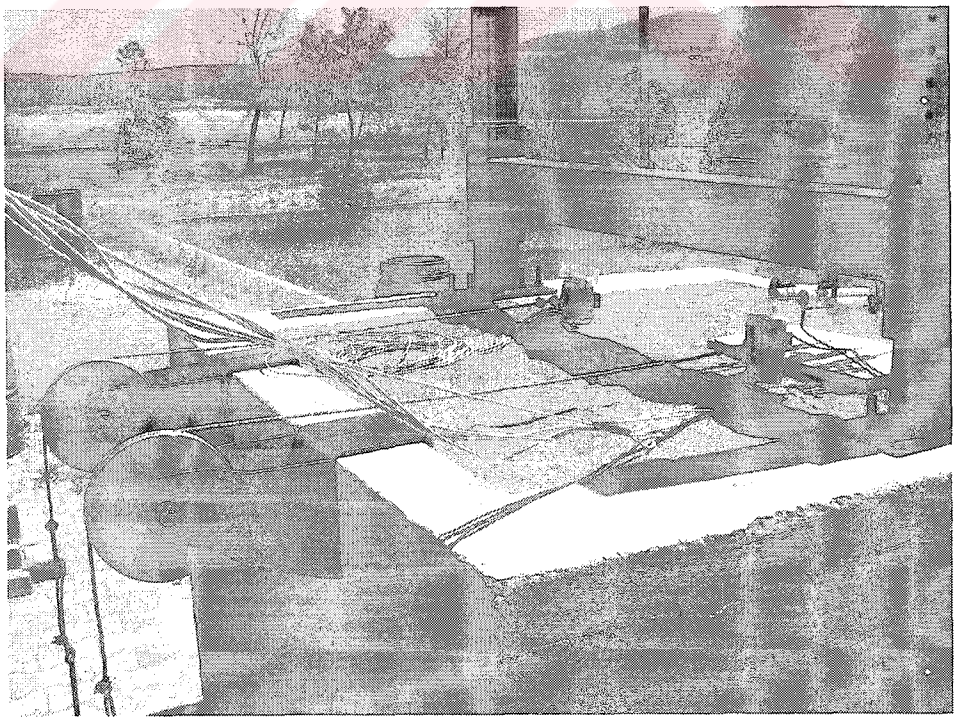

Figure 4.9 General view of the testing system prior to loading

4.3 General Soil Characteristics

The soil placed into the pool consists of bottom gravel and overlying sand layers. Major properties (i.e. relative density, specific gravity, and grain size distribution) of gravel and sand layers have been obtained by laboratory work. All tests were conducted according to ASTM standards. Wet sieve analysis test data for the gravel and sand layers are given in Table 4.1. Respective gradation curves are presented in Figure 4.10. Test results and classification of these soils are shown in Table 4.2.

Table 4.1 Sieve analysis data for gravel and sand layers

Sieve size	Gravel % passing by weight		Sieve size	Sand % passing by weight
1/2 in (13mm)	100			
3/8 in (10mm)	84.4			
No.4 (5mm)	29.1		No.4 (5mm)	100
No.8 (2.4mm)	14.8		No.10 (2mm)	91.6
No.16 (1.1mm)	7.4		No.30 (0.6mm)	57.3
No.30 (0.60mm)	5.4		No.60 (0.25mm)	23.8
No.50 (0.30mm)	3.4		No.80 (0.177mm)	14.3
No.100 (0.16mm)	0.9		No.140 (0.105mm)	7.6
No.200 (0.075mm)	0.6		No.200 (0.075mm)	6.2

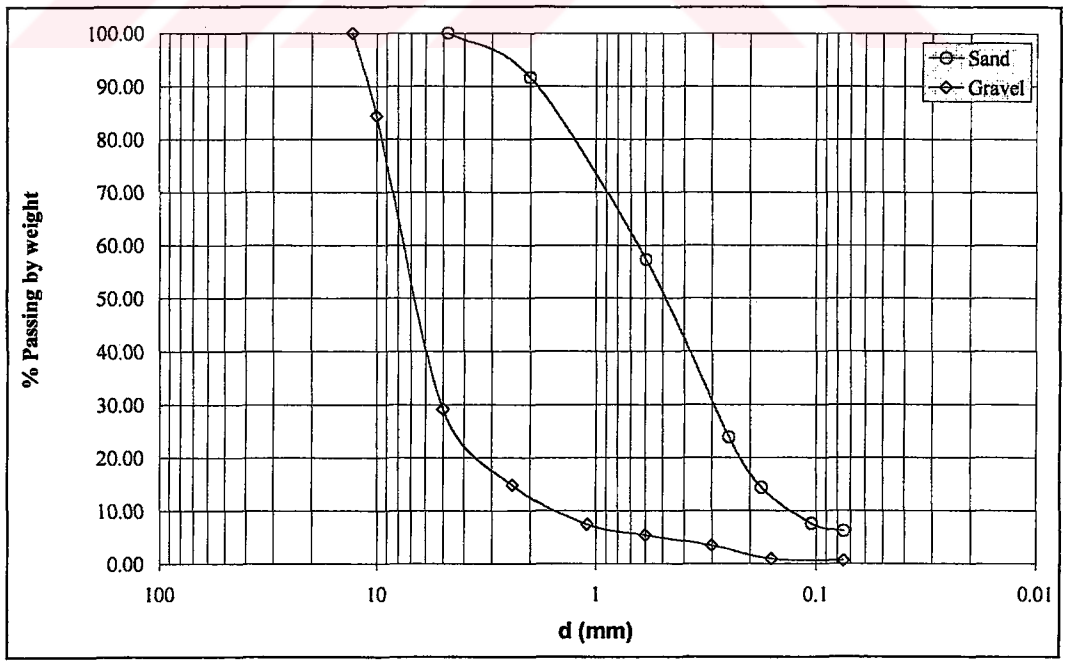

Figure 4.10 Grain size distribution curves of gravel and sand layers

Table 4.2 General soil characteristics

	γ_{max} (kN/m^3)	γ_{min} (kN/m^3)	G_s	C_u	C_c	-No.4	-No.200	USCS
Gravel	-	-	2.67	4.55	2.02	29.1	0.6	GW
Sand	19.2	16.6	2.65	4.68	0.92	100	6.2	SP-SM

The density of the sand layer would exert a significant effect on the performance of model piles. Therefore, average relative density of this layer should be determined using maximum, minimum and test average unit weight of the soil using Equation 4.3. . The unit weight of the sand layer during the test has been found by getting the weight of sand inserted in the pool. The weight of sand was obtained 17.16 kN and the volume of sand layer is 0.975m^3. So the average unit weight of sand was calculated γ=17.6 kN/m^3. The relatively density, D_r, has been found as %43 corresponding to medium dense condition. The angle of internal friction, however, was estimated using the below correlation between D_r and ϕ as given in Equation 4.4 (Bowles, 1996).

$$D_r = \frac{1/\gamma_{min} - 1/\gamma}{1/\gamma_{min} - 1/\gamma_{max}} \qquad 4.3$$

$$\phi = 28 + 15^o \cdot D_r \qquad 4.4$$

4.4 Data Acquisition System

In this experimental stress analysis study, PC-based data acquisition system was used in order to record induced strain in terms of potential difference, ΔE, calibrated with respect bending moment. Transducers at the pile head and strain gages along the model pile were used to measure the strain by detecting voltage change. Wheatstone Bridge configuration was necessary as signal conditioner in order to obtain regular voltage readings. Besides, the analog-to-digital signal converter (ADU) used in this study demands transducer type input rather than direct strain gage signals.

A typical Wheatstone Bridge consists of four resistive elements. In general single-arm bridges are normally employed for most experimental stress analysis

applications. The signal from the bridge may be amplified from 10 to 1000 times before recording. Therefore, a single active gage in position R_1 with a gage resistance of 120.0±0.4Ω was employed as illustrated in Figure 4.11. The resistances of R_2, R_3 and R_4 are also equal to 120.0Ω.

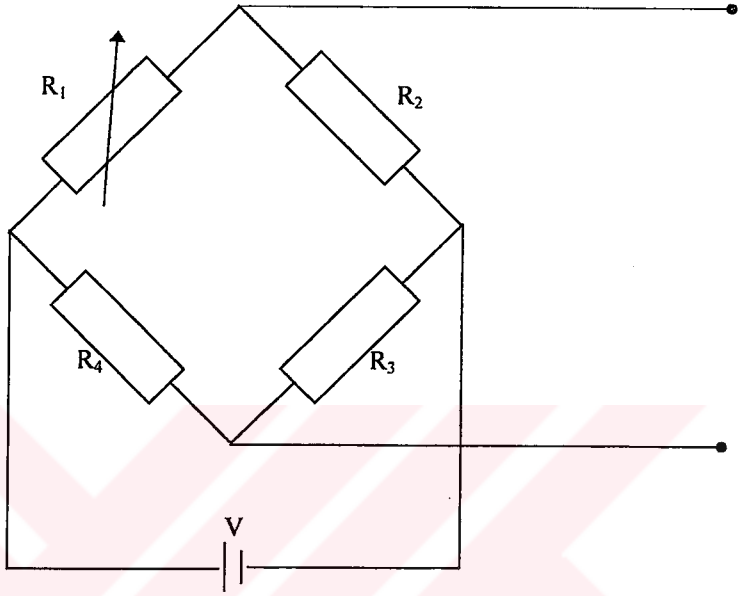

Figure 4.11 A view of Wheatstone Bridge

Voltage excitation source was able to supply 5 Volt to strain gages and transducers as shown in the flowchart of overall data acquisition system in Figure 4.12. Strain gages were connected to the bridge by shielded cable 4m in length as mentioned above, and the analog signal from bridges was also transferred by means of shielded cables. Total number of reading channels was eight. Five of these channels belong to strain gage bridges. Remaining three, however, were spared for displacement transducers. During lateral loading the pile bent producing analog signal, which was digitized and display simultaneously displayed on desktop monitor once it has reached to the computer through RS-232 COM communication port and processed by ADU software. As a consequence of this procedure pile head displacement and bending moment distribution along the pile were successfully established.

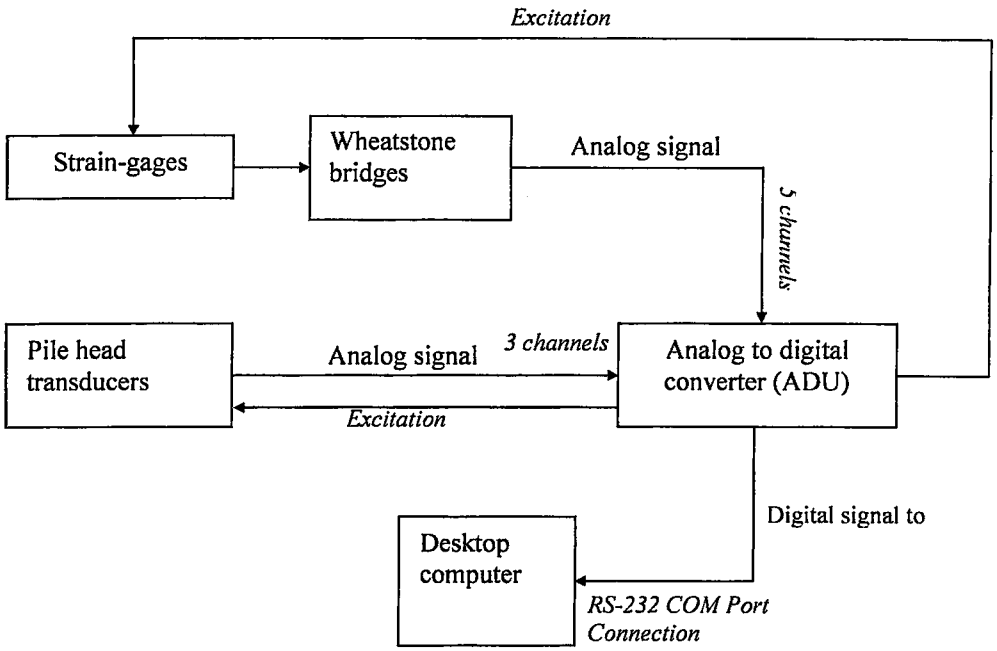

Figure 4.12 Data acquisition system

4.5 Calibration Procedure

Constant moment generation technique was used to develop a relationship between measured voltage and bending moment. A reinforced concrete model pile was used for this purpose. The reinforcing details of the calibration pile are given in Figure 4.13. The reinforcement is shown in Figure 4.14. One should note that special reinforcing was used in this relatively small-scale concrete pile. Strength tests of the selected material were performed prior to the design of the reinforcement configuration.

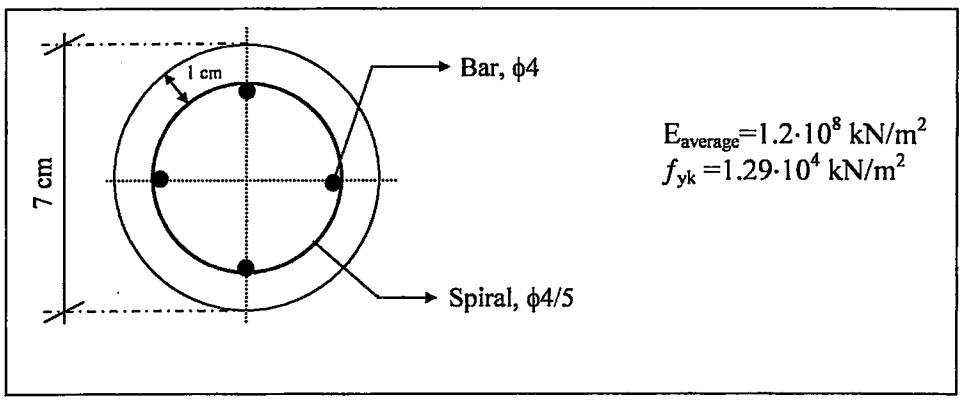

Figure 4.13 Reinforcement of calibration pile

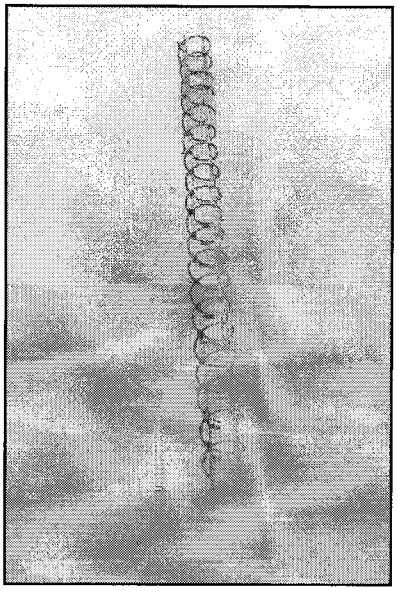

Figure 4.14 Reinforcement cage

The pile was simply supported with the moment producing vertical loads in the span were set 30cm apart as shown in Figure 4.15 and pictured in Figure 4.16. In order to generate pure bending moment condition the pile was loaded up to 35 kg on each load hanger. The load was increased at equal steps of 5 kg. Corresponding voltage changes were recorded by the data acquisition system during loading. Moment-voltage reading pairs were produced in this manner. Several loading-unloading-reloading cycles were performed. Separate calibration equations for forward loading and back loading cases were obtained as shown in Figures 4.17 and 4.18.

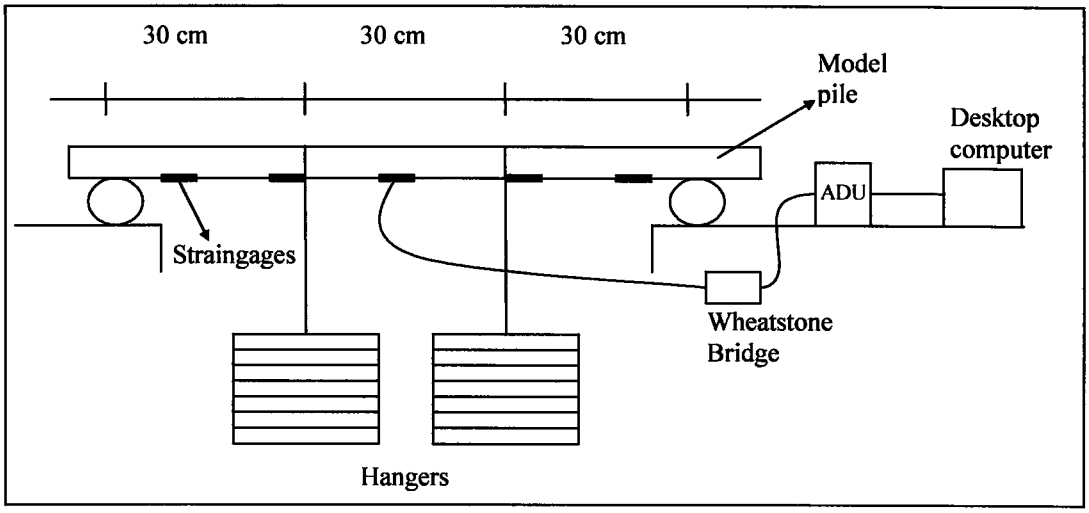

Figure 4.15 Strain gage calibration set-up

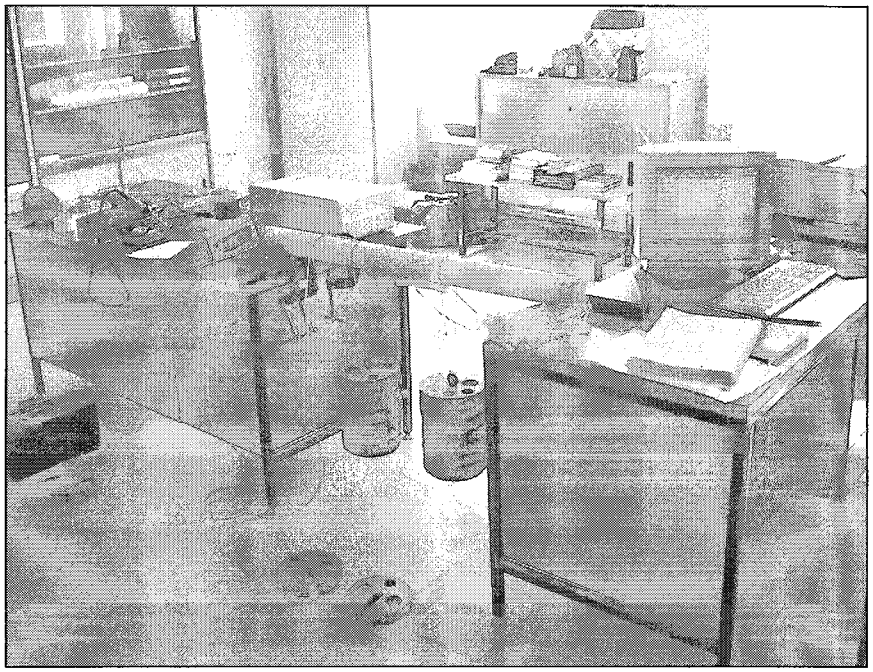

Figure 4.16 Strain-gage calibration system view

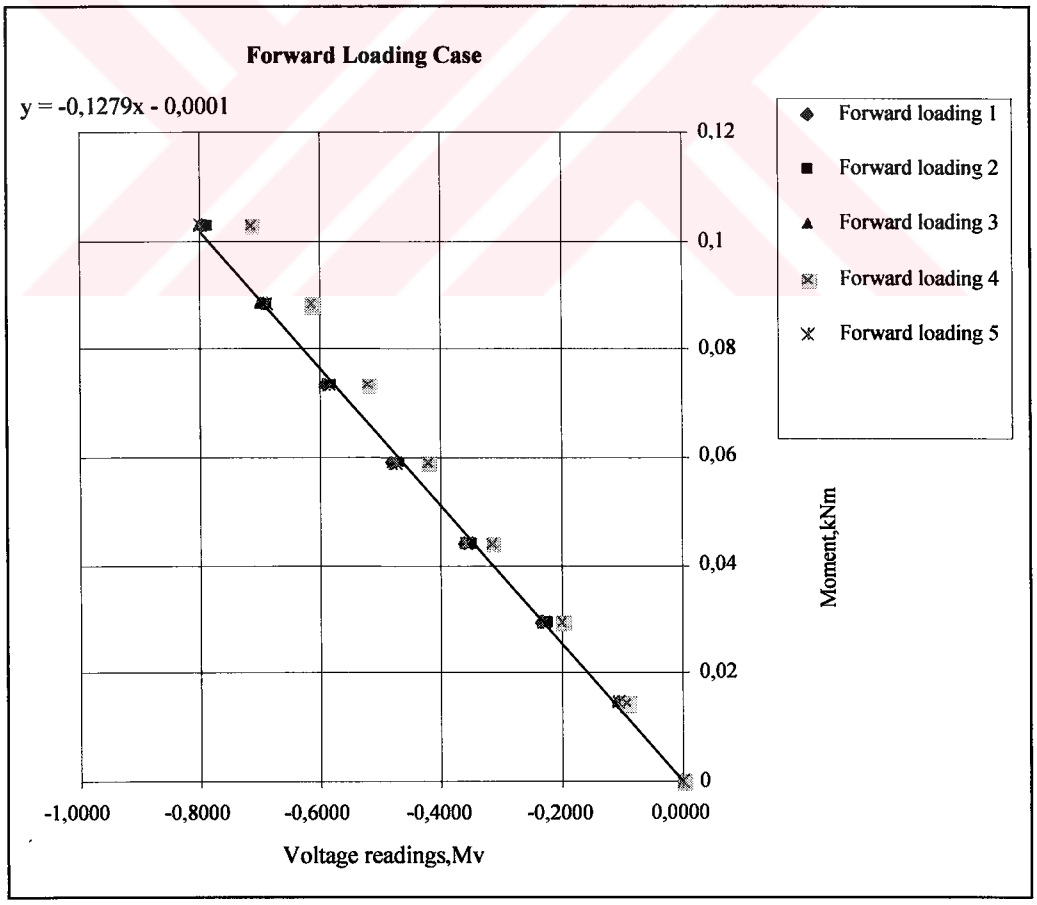

Figure 4.17 Moment calibration equation of for forward loading

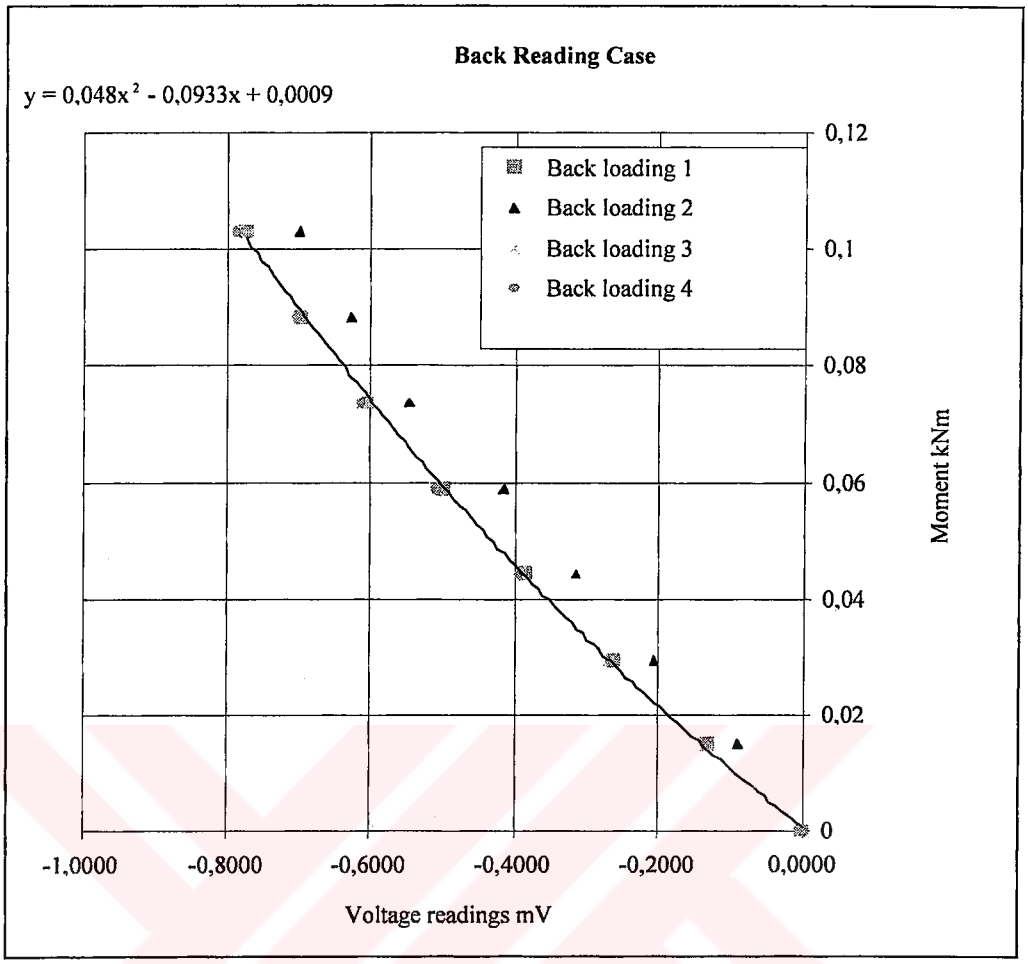

Figure 4.18 Moment calibration equation of for backward loading

CHAPTER FIVE
CONCRETE MIX DESIGN

5.1 Introduction

Steel fibers improve the ductility of concrete under all modes of loading. However, their effectiveness in improving strength varies among compression, tension, shear, torsion, and flexural loading cases. This research study aims to understand mechanisms of lateral loading capacity changes for SFRC piles. Therefore, improvement of flexural strength is thought as a major governing parameter of model piles. The flexural strength of steel fiber reinforced concrete, however, increases by 50 to 70 percent in comparison with the performance of unreinforced conventional concrete produced without admixtures. During the course of the study material control tests were planned and performed prior to the casting of the model piles to make sure that consistent concrete production with and without steel fibers could be confidently made. Needless to say it was desirable to obtain notable improvements in the behavior of the SFRC with respect to the conventional concrete. In the following experimental work is briefly explained and the design of the concrete mix for both conventional and SFRC cases is presented.

5.2 Experimental Program

Several concrete materials laboratory tests were performed to determine the flexural strength, compressive strength, and modulus of elasticity of steel fiber reinforced (SFRC) and conventional concrete. The tests performed to reach the goals of this part of the research can be listed as in the following:

a. Compressive strength test

b. Third-point bending moment test
c. Air content determination
d. Conventional slump test
e. Inverted slump cone test
f. Specific gravity determination
g. Sieve analysis test
h. Percent absorption determination

The above listed tests were all performed in accordance with ASTM standards.

5.3 Characteristics of Materials and Concrete Mix

A 1/2" (12.5mm) maximum-size aggregate was selected, as it is less than the one fifth of the model pile diameter. Particle size range of the coarse and fine fractions of the aggregate mixture was 5-12.5mm and 0-5mm, respectively. Percent absorption test was especially important for the control of net water content of the concrete mix so that determination of correct batch weights would be made. The specific gravity values were used in certain computations for mixture proportioning and control, such as the absolute volume occupied by the aggregate.

Table 5.1 Characteristics of aggregate fractions

Aggregates (mm)	Absorption (%)	Oven-dry specific gravity	Saturated dry surface specific gravity
5-12.5	0.58	2.66	2.68
0-5	1.21	2.59	2.62
Sand	1.63	2.56	2.60

Gradation of aggregates significantly affects concrete mixture proportioning and workability. The grading of aggregates has been determined by means of sieve analysis test. Then mixture proportions of the aggregate fractions were decided according to ACI 544.1R-8; (*Table 2.1-Recommended combined aggregate gradations for steel fiber reinforced concrete*). The gradation of the combined aggregate, which was generated due to ACI recommendations, is shown in Figure 5.1. As can be noticed in this figure ACI limits are satisfied with this mixture.

Table 5.2 Particle size distribution

Sieve size	Aggregate Fraction		
	5-12.5	0-5	Sand
½ in (13mm)	99	100	100
3/8 in (10mm)	84.4	100	100
No.4 (5mm)	29.1	98.8	99.7
No.8 (2.4mm)	14.8	72.9	77.3
No.16 (1.1mm)	7.4	46.2	47.3
No.30 (0.60mm)	5.4	26.5	25.7
No.50 (0.30mm)	3.4	13.1	9.4
No.100 (0.16mm)	0.9	3.1	4.3
No.200 (0.075mm)	0.6	1.1	0.8

Table 5.3 Mixture proportions of the aggregate

Fraction	Mixture proportions, %
5-12.5	35
0-5	55
Sand	10

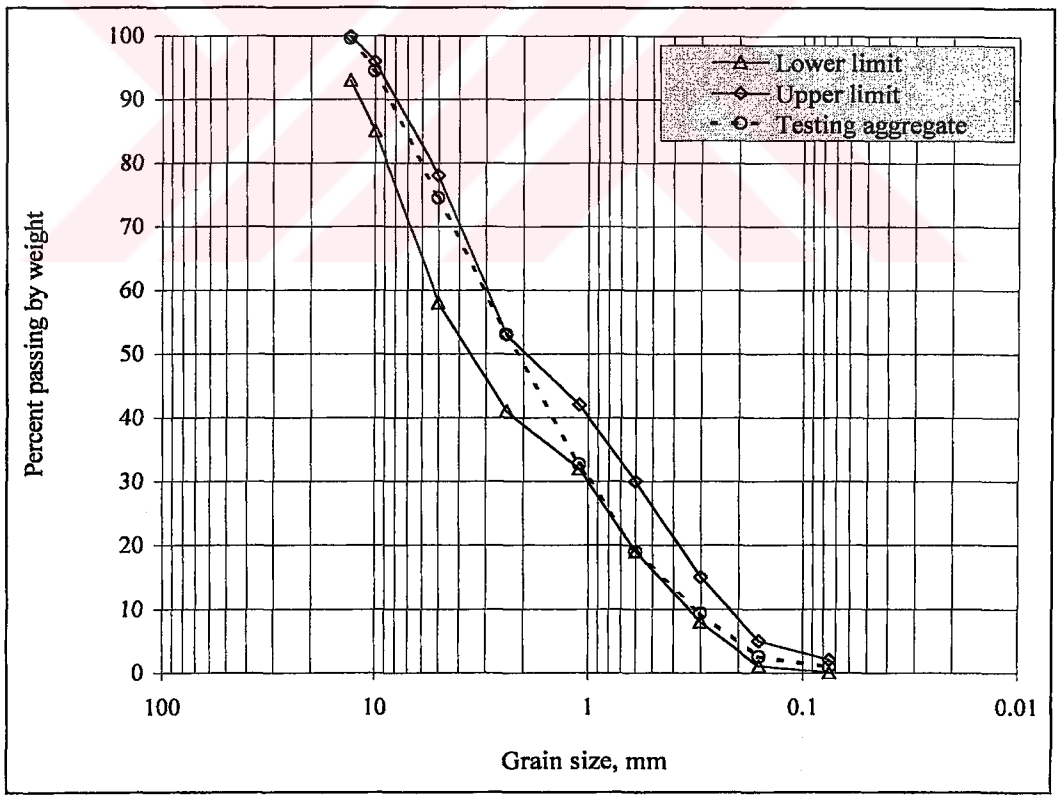

Figure 5.1 Combined aggregate gradation within the ACI recommended limits

Portland cement type CEM I 42.5R has been used in concrete mix. The cement manufacturer has reported specific gravity of the cement as 3.1. Water cement ratio

(w/c) has been decided to provide 3 to 4" (7.62mm to 10.16mm) slump (Kosmatka, H.& Panarese, 1994 - *Design and Control of Concrete Mixtures, Table 7.7 and Table 7.6, page 81).*

Table 5.4 Recommended slumps for various types of construction. ***(Table 7.7 page 81)***

Concrete construction	Slump in (cm)	
	Maximum	Minimum
Reinforced foundation walls and footings	***3 (7.62)***	***1 (2.54)***
Plain footings caissons and substructure walls	3 (7.62)	1 (2.54)
Beams and reinforced walls	4 (10.16)	1 (2.54)
Building columns	4 (10.16)	1 (2.54)
Pavements and slabs	3 (10)	1 (2.54)
Mass concrete	2 (5.08)	1 (2.54)

It appears that the bold marked line in Table 5.4 (i.e. reinforced foundation walls and footings) better fits to model pile test research. This option requires the slump to be 3 to 4 inches (7.62cm to 10.16cm) for non-air-entrained concrete with ½in maximum size aggregate. Therefore, slump was estimated to be approximately 4 in (10.16mm) for the batch design. Batch characteristics of SFRC with respect to the maximum size aggregate are shown in Table 5.5. Having maximum aggregate size equal to 12.5mm the 3/8" (10mm) option has been decided to form the basis for SFRC design in this study. It should be noted that upper limit of the water to cement ratio was selected since it was afraid that lower values would end up producing to stiff SFRC batches.

Table 5.5 Range of normal weight SFRC (ACI, 1996)

Mix parameter	Maximum Size Aggregate		
	3/8" (10mm)	3/4" (19mm)	1.5" (38mm)
Cement, kg/m^3	356-593	297-534	279-415
Water-cement ratio, w/c	0.35-0.45	0.35-0.50	0.35-0.55
Percent of fine total aggregate	45-60	45-55	40-55

Table 5.6 was used for selecting air content of the batch. Therefore, corresponding amounts for water and cement were automatically used in the batch design.

Table 5.6 Trial mixtures for non-air-entrained concrete of medium consistency Slump: 3" to 4"-7.62mm to 10.16mm, (Kosmatka,H.&Panarese, 1994)

Water -cement ratio	Maximum size of aggregate in.(mm)	Air content percent	Water lb per cubic yd (kg per cubic meter) of concrete	Cement lb per cubic yd (kg per cubic meter) of concrete
0.45	3/8 (10mm)	3	385(228.28)	855(506.96)
	1/2 (13mm)	**2.5**	**365(216.12)**	**810(480.27)**
	3/4 (19mm)	2	340(201.60)	755(447.66)
	1 (25mm)	1.5	325(192.70)	720(426.91)
	1.5 (38mm)	1	300(177.88)	665(394.30)

5.4 Mixture Proportioning

Proportioning methods have evolved from the arbitrary volumetric method of the early 1900's to the present day weight and absolute-volume methods described in the American Concrete Institute's Committee 211-*Standard Practice for Proportioning Concrete Mixes.* The volumetric method is said to be more accurate (Kosmatka & Panarese, 1994). Therefore, absolute volumetric method was used in this study. This method is explained in the following:

Absolute volume: The volume of freshly mixed concrete is equal to the sum of the absolute volumes of the cement, water (excluding the water present in aggregate voids), aggregate and air. The absolute volume is computed from the material weight and the specific gravity as follows:

$$Absolute\ volume = \frac{Weight\ of\ material}{Specific\ gravity\ of\ material \cdot Unit\ weight\ of\ water}$$

Volume computations per 1000 dm^3 become:

$V_{water} = 216.123\ dm^3$

$V_{air} = 25\ dm^3$

$V_{cement} = 480.274/(3.1) = 154.927\ dm^3$

$\Rightarrow \Sigma V = 396.05\ dm^3 / m^3$

$\Rightarrow V_{aggr.} = 1000 - 396.05 = 603.950\ dm^3 / m^3$

The specific gravity of the oven-dry aggregate was used to performe mixture design. The weight of dry aggregate was calculated as follows:

$W_{dry-aggr.} = Mixture\ proportion \cdot V_{aggr.} \cdot Oven\ dry\ specific\ gravity_{aggr.}$

Example calculation for aggregate type 5-12.5mm:

$W_{dry-aggr.} = 0.35 \cdot 603.950 \cdot 2.66 = 562.28\ kg / m^3$ (See Table 5.7 below)

Table 5.7 The weight of dry aggregate (kg per one cubic meter of mixture)

Aggregate	Mixture proportions, %	Oven-dry specific gravity	Dry aggregate weight
5-12.5	35	2.66	562.28
0-5	55	2.59	860.33
Sand	10	2.56	154.61

The mixture then has the following proportions before production of trial mix for one cubic meter of concrete.

$W_{water} = 216.123\ kg$

$W_{cement} = 480.274\ kg$

$W_{5-12.5} = 562.280\ kg$

$W_{0-5} = 860.330\ kg$

$W_{sand} = 154.61\ kg$

$\Sigma W = 2273.617\ kg / m^3$

Target slump : 4 in. (10.16cm)

Target air content : 2.5%

The above given mix characteristics belong to the design concrete mix without moisture correction. This correction, however, is an important aspect of batch design.

Application of moisture correction to design parameters is given for a trial batch study in the following.

5.5 Trial Batch

Trial batches should be casted in order to verify target slump and air content would be successfully obtained. The necessary steps in trial batch design are given in subsequent sections. The volume of this batch has been decided as 35 dm^3.

5.5.1 Moisture Correction

In practise aggregate grains contain some measurable amount of moisture. Corrections are needed to compensate for moisture changes in the aggregate. The dry-batch weight of the concrete aggregate therefore has to be adjusted to compensate for any detected moisture variations due to absorbed or surfacial water of individual grains. The mixing water added to the batch must be reduced or increased by the amount of moisture change of the aggregate. Such corrections were inevitably made for the batches produced in this study. The moisture content of aggregate fractions was determined before the trial batch has been casted. It should be mentioned that conventional oven was used for moisture content determination since more stable values were obtained. Results are given in Table 5.8.

Table 5.8 Moisture content test results.

Aggregate	Moisture content, w (%)
5-12.5	0.052
0-5	1.134
Sand	1.920

Note that dry weights are increased properly to account for moisture content as in the following:

$$W_{5-12.5} = 562.280 \cdot (1 + 0.052\%) = 562.572\ kg$$

$$W_{0-5} = 860.330 \cdot (1 + 1.134\%) = 870.086\ kg$$

$$W_{sand} = 154.610 \cdot (1 + 1.920\%) = 157.579\ kg$$

Absorbed water does not become part of the mixing water and must be excluded from the water adjustment:

$$\Delta w_{5-12.5} = 0.052\% - 0.58\% = -0.528\%$$

$$\Delta w_{0-5} = 1.134\ \% - 1.21\ \% = -0.076\ \%$$

$$\Delta w_{sand} = 1.920\ \% - 1.63\ \% = 0.29\ \%$$

Final amount of free water to be used in the trial batch can be calculated as:

$$W_{free-water} = 216.123 - (-0.528\ \&\ \% \cdot 562.280 + (-0.076\%) \cdot 860.33 + (0.29\%) \cdot 154.610)$$
$$= 219.297\ kg/m^3$$

Corrected batch weights can be listed as:

$$W_{water} = 219.123\ kg$$

$$W_{cement} = 480.274\ kg$$

$$W_{5-12.5} = 562.572\ kg$$

$$W_{0-5} = 870.086\ kg$$

$$W_{sand} = 157.579\ kg$$

$$\Sigma W = 2289.741\ kg/m^3$$

Trial batch has been casted with above proportions. Air content has been found as 2.3% at 1.5 atm. Air content of the concrete was calculated as follows:

$$A_s = A_1 - G$$

where:

A_s = air content of the sample, %

A_1 = apparent air content of the sample, % (2.7%)
G = aggregate correction factor, % (0.4%)

The slump of this batch has been measured as 6 cm.

5.5.2 Batch Adjustments

The measured 6 cm slump cannot be accepted since the allowed margin for the slump difference between realized and target slump is max.1.9 cm. The batch happened to stiffer than desired. Measured air content of 2.3% was also less than the target value of 2.5%.

It is customary to expect that decreasing the mixing water by 5 lbs (2.27 kg) should end up increasing air content by 1%. Similarly increasing the water content by 10 lbs (4.54 kg) the slump is increased by 1 inch (2.54 cm).

The adjusted water to increase slump and air content by necessary amount to reach target values can be found as:

$$W_{water-adjust} = ((4.54 \cdot (10.16 - 6)/2.54) - (2.27 \cdot (2.5\% - 2.3\%)) = 6.99\, kg$$

The new batch weights based on the new water content are calculated as follows:

$$W_{water} = 216.123 + 6.99 = 223.113\, kg$$

Since water weight has been as a result of adjustments, cement weight was also recalculated for w/c = 0.45.

$$\Rightarrow W_{cement} = 223.113/0.45 = 495.81\, kg$$

Volume computations per 1000 dm^3 are as fallows:

$$V_{water} = 223.113\, dm^3$$

$$V_{air} = 25 \ dm^3$$

$$V_{cement} = 495.81/(3.1) = 159.94 \ dm^3$$

$$\Rightarrow \Sigma V = 408.052 \ dm^3 / m^3$$

$$\Rightarrow V_{aggr.} = 1000 - 408.052 = 591.9408 \ dm^3 / m^3$$

Adjusted aggregate weights are given in Table 5.9.

Table 5.9 Adjusted aggregate proportions per one cubic meter

Aggregate	Mixture proportions, %	Oven dry specific gravity	W_{dry} (kg/m^3)
5-12.5	35	2.66	551.104
0-5	55	2.59	843.230
Sand	10	2.56	151.539

Final adjusted batch weights per cubic meter of concrete:

$$W_{water} = 223.123 \ kg$$

$$W_{cement} = 495.81 \ kg$$

$$W_{5-12.5} = 551.104 \ kg$$

$$W_{0-5} = 843.230 \ kg$$

$$W_{sand} = 151.539 \ kg$$

$$\Sigma W = 2264.806 \ kg / m^3$$

5.6 SFRC Mixture Proportioning

Same principals apply to SFRC design except that the volume of steel fiber to be used in the batch results in a reduction in the volume of sand. Sample SFRC design calculations are given for ZP305 (aspect ratio: 30/0.5) with a volume ratio of 1.5%. Note that this ratio has been selected for control batch and quality control tests.

Volumetric computations per 1000 dm^3 are as follows for SFRC:

$$V_{aggr.} = 591.948 \ dm^3$$

$V_{sand} = 10\% \cdot 591.948 = 59.195\ dm^3$

$V_{steel\ fiber} = 15\ dm^3$

$V_{sand-SFRC} = 59.195 - 15 = 44.195\ dm^3$

The dry weight computations are as follows:

$W_{sand} = 44.195 \cdot 2.56 = 113.139\ kg$

$W_{fiber} = 15 \cdot 7.8 = 117\ kg$

Batch weights per cubic meter of steel fiber reinforced concrete obtained as follows:

$W_{water} = 223.123\ kg$

$W_{cement} = 495.81\ kg$

$W_{5-12.5} = 551.104\ kg$

$W_{0-5} = 843.230\ kg$

$W_{sand} = 113.139\ kg$

$W_{fiber} = 117\ kg$

$\Sigma W = 2343.406\ kg/m^3$

5.7 Concrete Tests

Compressive strength can be defined as the measured maximum resistance of a concrete specimen to axial loading. For each type of concrete 35 dm^3 batch was prepared. The aggregates were mixed first. Then fibers were added slowly as the mixer was rotating. Finally cement and water were added and mixed until fibers get separated. Once the batch was mixed up properly slump and air content tests were performed first. Conventional slump test was used for control concrete whereas both conventional and inverted slump tests were made for SFRC. Compared with conventional concrete, SFRC includes higher cement and fine aggregate in addition

to fibers. Hence addition of fiber decreases the slump of the concrete. Therefore, conventional slump test is not appropriate for SFRC. It is recommended for most SFRC applications to conduct inverted slump test, which requires measurement of the time necessary for the consolidation of the sample by means of mechanical vibration (ACI, 1996). Slump and air content values for the tested samples are shown in Table 5.10.

Table 5.10 Fresh concrete properties of compressive strength test specimens

Properties		Control concrete	SFRC
Air content (%)		2.5	2.6
Slump	Conventional method (cm)	10.20	4.0
	Inverted slump cone test (sec)	-	8.0

The uniaxial compression tests were made using SFRC and control concrete cylinder specimens 10 cm in diameter and 20 cm in height. Cylindrical specimens were compacted using vibration table technique. Specimens were taken out of their moulds 24 hours later and cured in water. Tests were performed at 7, 14, and 28 day curing times. Test rate was 2.35 kN/sec. Table 5.11 gives compression test results.

Table 5.11 Compressive strength test results

Dimensions Diameter:10cm Length : 20cm		$f_{c\text{-}7}$ (Mpa)	$f_{c\text{-}14}$ (Mpa)	$f_{c\text{-}28}$ (Mpa)
Control concrete	Sample 1	35.16	39.47	40.87
	Sample 2	34.93	40.13	37.59
	Sample 3	34.79	40.37	-
	Average	**34.92**	**39.99**	**39.23**
SFRC (Fiber: 1.5%)	Sample 1	36.00	35.85	40.28
	Sample 2	35.22	38.62	40.72
	Sample 3	33.96	37.31	42.15
	Average	**35.06**	**37.26**	**41.05**

As one notice in the above tables target slump and air content values were successfully obtained in laboratory tests indicating satisfactory SFRC and conventional concrete mix designs. The compressive strength, f_c, of both type

concrete specimens (i.e. conventional and SFRC with 1.5% fiber) did not differ significantly as expected. It was stated that addition of steel fibers into the concrete would not alter compressive strength considerably (ACI, 1996). Achieved concrete can be classified as C40. Flexural strength of SFRC and conventional concrete specimens were determined using third-point loading technique. Specimens were casted using prismatic moulds $10 \times 10 \times 60$ cm. The volume of each batch was 80 dm^3. Slump and air content values for these batches are given in Table 5.12.

Table 5.12 Fresh concrete properties of flexural strength test specimens

Properties		Control concrete	SFRC
Air content (%)		2.5	2.5
Slump	Conventional method (cm)	12.0	3.8
	Inverted slump cone test (sec)	-	6.0

Test specimens were compacted on a vibrating table. Specimens were taken out of their moulds 24 hours later and cured in water. Tests were performed at 7, 14, and 28 day curing times. Testing rate was 0.20 kN/sec. The testing system was a closed loop servo-hydraulic universal testing machine. Flexural strength test results are given in Table 5.13.

Table 5.13 Flexural strength test results

Dimension 10 x 10 x 60 cm		f_{ct-7} (MPa)	f_{ct-14} (MPa)	f_{ct-28} (MPa)
Control concrete	Sample 1	4.83	5.85	5.85
	Sample 2	5.65	5.68	6.58
	Sample 3	5.08	5.54	5.98
	Average	**5.19**	**5.69**	**6.14**
SFRC (Fiber: 1.5%)	Sample 1	5.80	6.76	7.35
	Sample 2	6.32	6.67	6.85
	Sample 3	6.14	6.41	7.15
	Average	**6.09**	**6.61**	**7.12**

Similar to compressive strength test specimen batch properties satisfactory slump and air content values were obtained for flexural test specimen batches. In the literature it is stated that steel fibers are able to improve flexural strength of the

concrete as much as 40~60% (ACI, 1996). It can be noticed in Table 5.13 that detected increase of flexural strength for a fiber volume fraction of 1.5% is 16.0% on the average. Although this amount is lower than the reported, it is thought that low fiber aspect ratio and small maximum aggregate size are responsible for this. It should be kept in mind that fiber type has got one of the lowest possible aspect ratio (l/d=60) values available in the market. Besides, model pile diameter has dictated selection of small maximum aggregate size (12.5 mm). It is believed that use of fiber with higher aspect ratio and appropriate mix design would result in higher flexural strength increase.

CHAPTER SIX
RESULTS and DISCUSSIONS

6.1. Introduction

A total of ten piles were cast as mentioned in the second chapter. However, four types of model piles could be tested during this thesis study. Some unexpected circuit failures in the electronic data acquisition system caused serious delays in the testing schedule. Therefore four model pile tests could have been conducted successfully. The list of the tests is given in Table 6.1.

Table 6.1 Model pile tests

Test #	Material	Fiber Content
1	Concrete	-
2	SFRC	1.5% (ZP305)
3	SFRC	1.0% (ZP305)
4	SFRC	0.75% (ZP305) + 0.25% (micro fiber)

6.2. Test #1: Concrete Model Pile

In this test a concrete pile without any reinforcement and steel fibers was tested. During the test loading was applied at 5 kg increments. An unloading branch was made when the load reached to 30 kg. Once the pile was completely unloaded a reloading was made until the pile was broken at 70 kg. The pile head transducers and strain-gages along the pile generated continuous data through out the test. It was observed that the pile behaved quite breaking at a point 39cm below the top of the

pile. Total pile head displacement was measured as 1.208 mm. It should be mentioned that the pile was suddenly pulled out of the sand just after loaded with 80 kg. Evaluation of the data showed that moment readings were meaningless past 70 kg. The pile head displacement-lateral load and distribution of the moment along the pile graphs are given in Figures 6.1 and 6.2, respectively. General view of the test set-up just after the pullout of the broken pile is shown in Figure 6.3. The broken pile after the test is shown in Figure 6.4.

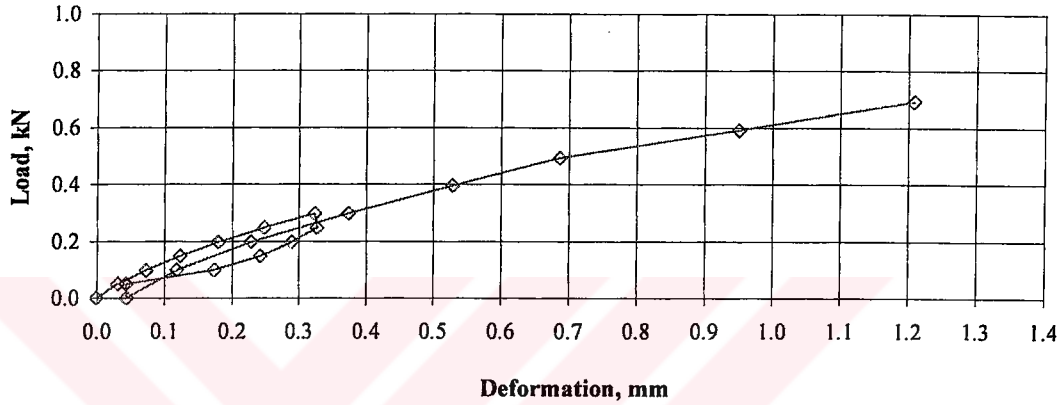

Figure 6.1 Pile head displacement for Test #1

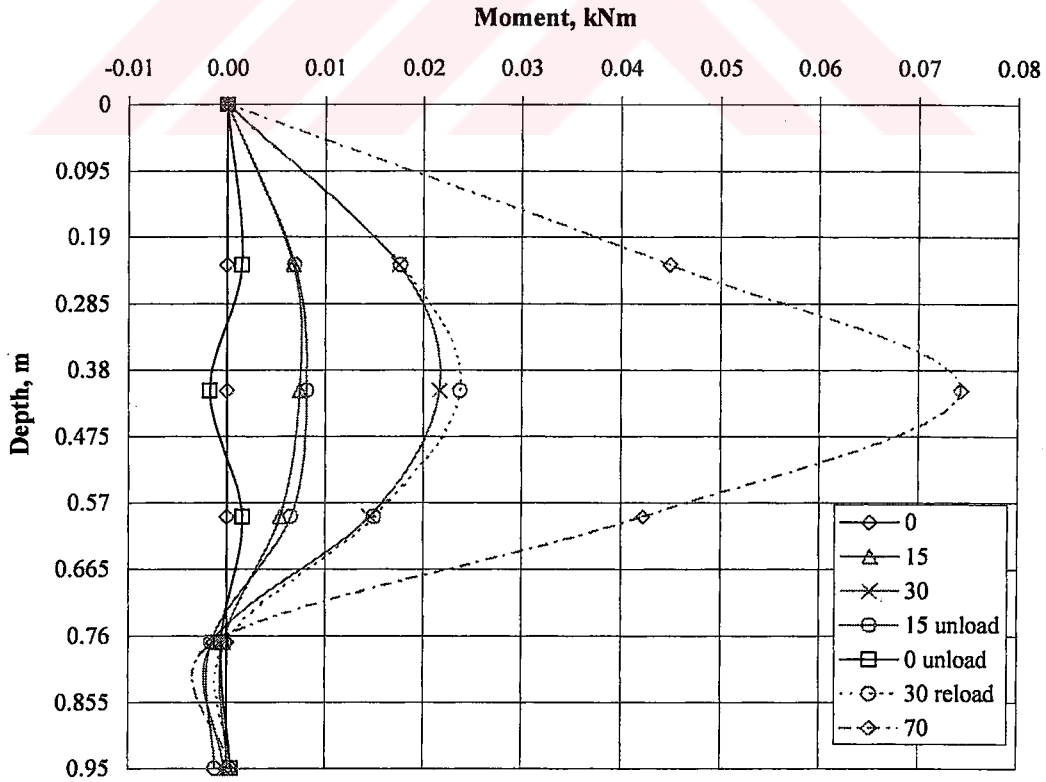

Figure 6.2 Moment distribution for Test #1

Figure 6.3 General view at the end of the Test #1

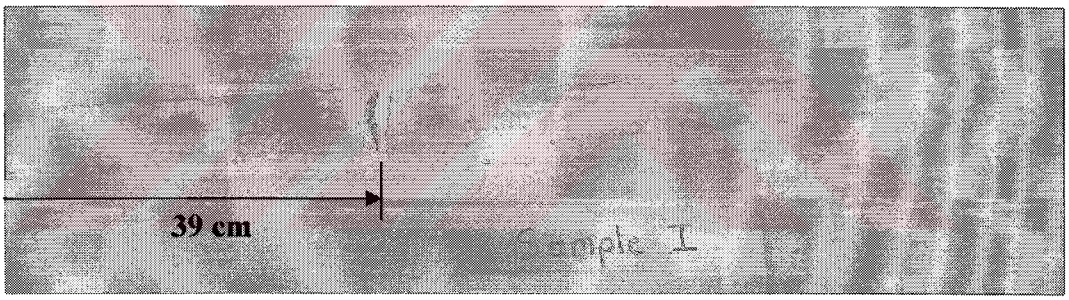

Figure 6.4 General view of the broken pile of the Test #1

6.3. Test #2: SFRC Model Pile with 1.5% ZP305 Steel Fiber

In this test a SFRC pile with a volume content of %1.5 steel fiber was tested. Above-mentioned unloading and reloading procedure was also applied in a similar manner. The pile was unloaded when the static load was at 30 kg and 60 kg. It was observed that the pile behaved quite flexibly with the formation of two plastic hinges at 44.5 cm and 27 cm depths below pile top. The pile achieved ultimate lateral load capacity of 130kg beyond which the fibers were completely pulled out of the concrete at the upper plastic hinge. Had the load not been increased up to 130 kg, the

second plastic hinge would have stayed stationary without transferring bending moment to the lower strain gages. This fact is also explained on the respective graph. Total pile head displacement was measured as 8.46 mm. Evaluation of the data showed that moment readings were meaningless past 130 kg. The pile head displacement-lateral load and distribution of the moment along the pile graphs are given in Figures 6.5 and 6.6, respectively. General view of the test set-up just after the pullout of the broken pile is shown in Figure 6.7. The broken pile after the test is shown in Figure 6.8.

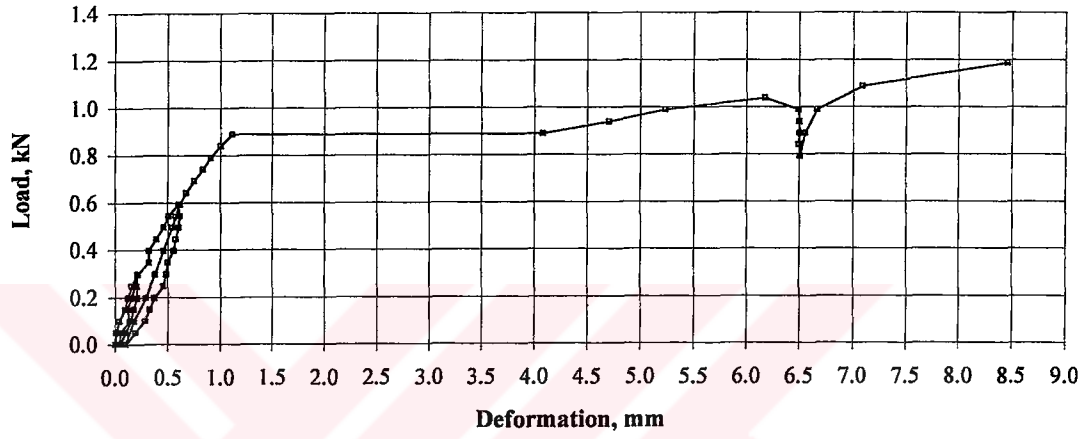

Figure 6.5 Pile head displacement for Test #2

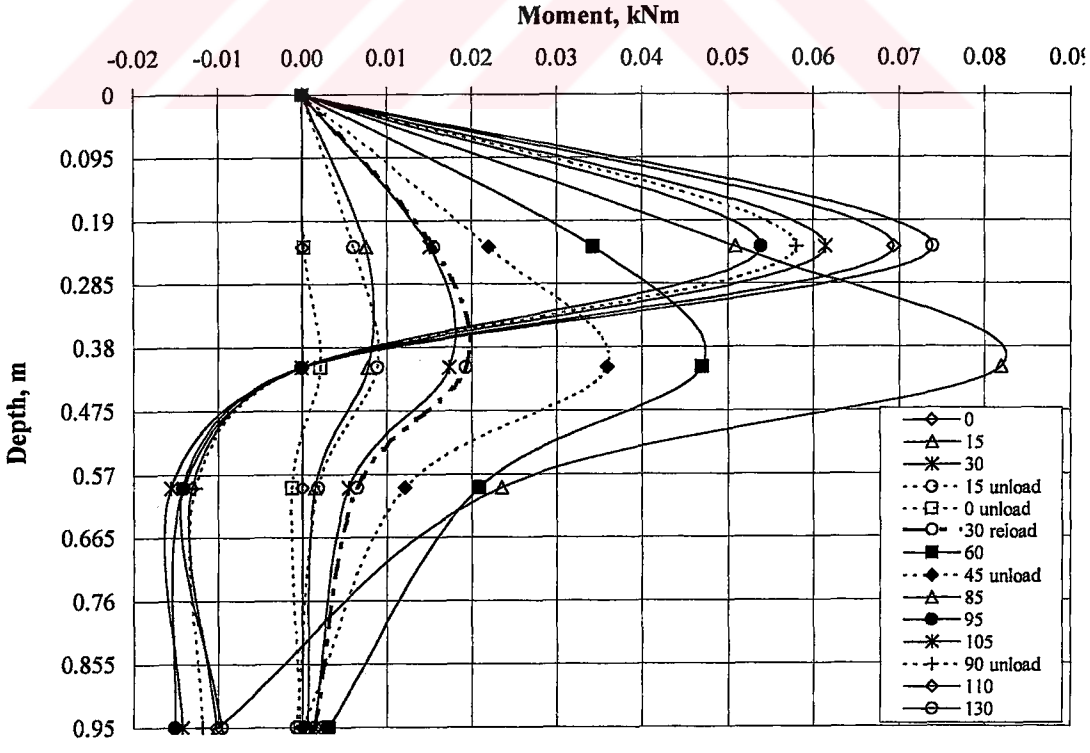

Figure 6.6 Moment distribution for Test #2

Figure 6.7 General view at the end of the Test #2

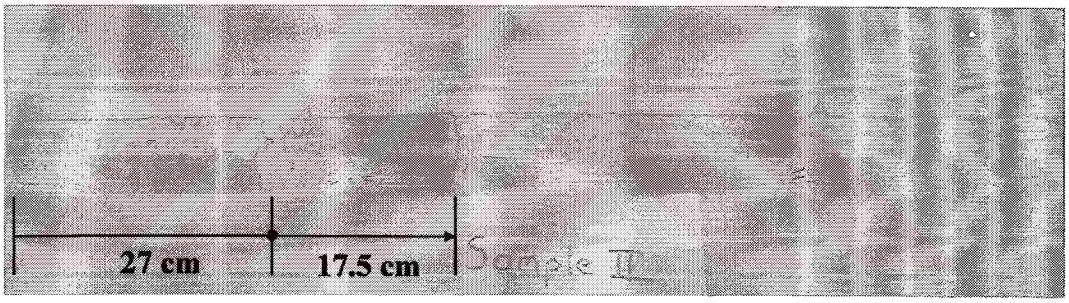

6.8 General view of the broken pile of the Test #2

6.4. Test #3: SFRC Model Pile with 1.0% ZP305 Steel Fiber

In this test a SFRC pile with a volume content of %1 steel fiber was tested. The pile was similarly unloaded when the static load was at 30 kg and 60 kg. It was observed that the pile behaved quite flexibly with the formation of two plastic hinges at 47 cm and 29 cm depths below pile top. Note that the behavior of pile and plastic hinge positions are similar to the previous model pile with 1.5% fiber. However, the ultimate load capacity of Test #3 pile was 1.08 times larger than that of the Test #2 pile. Reaching ultimate load capacity at 145 kg, fibers of the model pile in Test #3 were pulled out similar to those in Test #2. Total pile head displacement was

measured as 5.9 mm. But this pile head deformation value has been recorded at 90 kg. Unfortunately further readings could not be obtained for some reason. On the other hand, recorded final head deformation value (5.9 mm) indicates that overall pile head deformation would have been quite large. The pile head displacement-lateral load and distribution of the moment along the pile graphs are given in Figures 6.9 and 6.10, respectively. General view of the test set-up just after the pullout of the broken pile is shown in Figure 6.11. The broken pile after the test is shown in Figure 6.12.

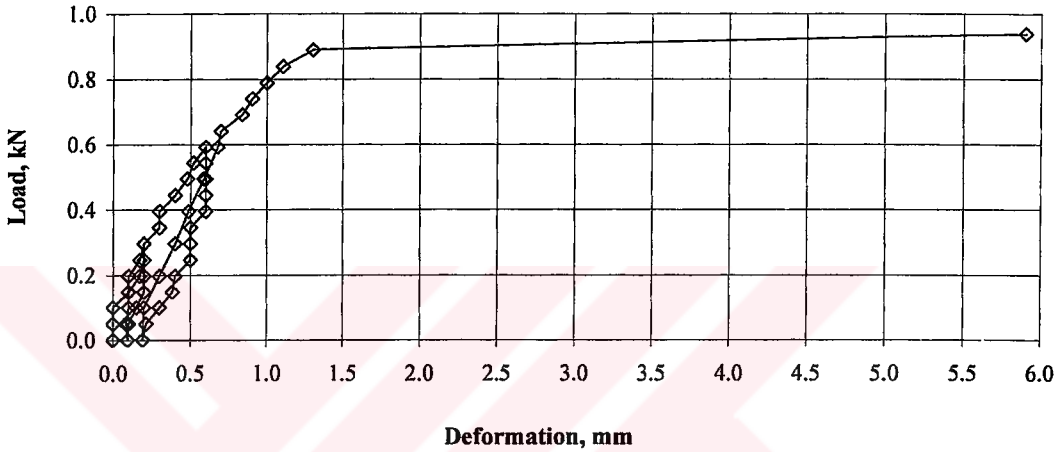

Figure 6.9 Pile head displacement for Test #3

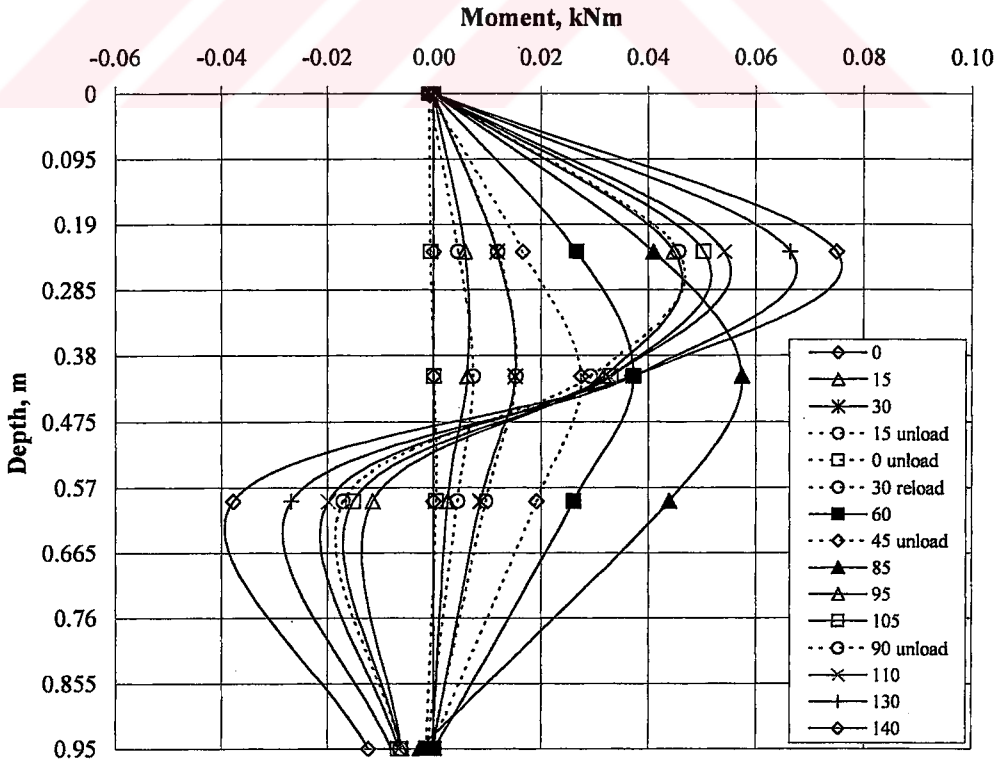

Figure 6.10 Moment distribution for Test #3

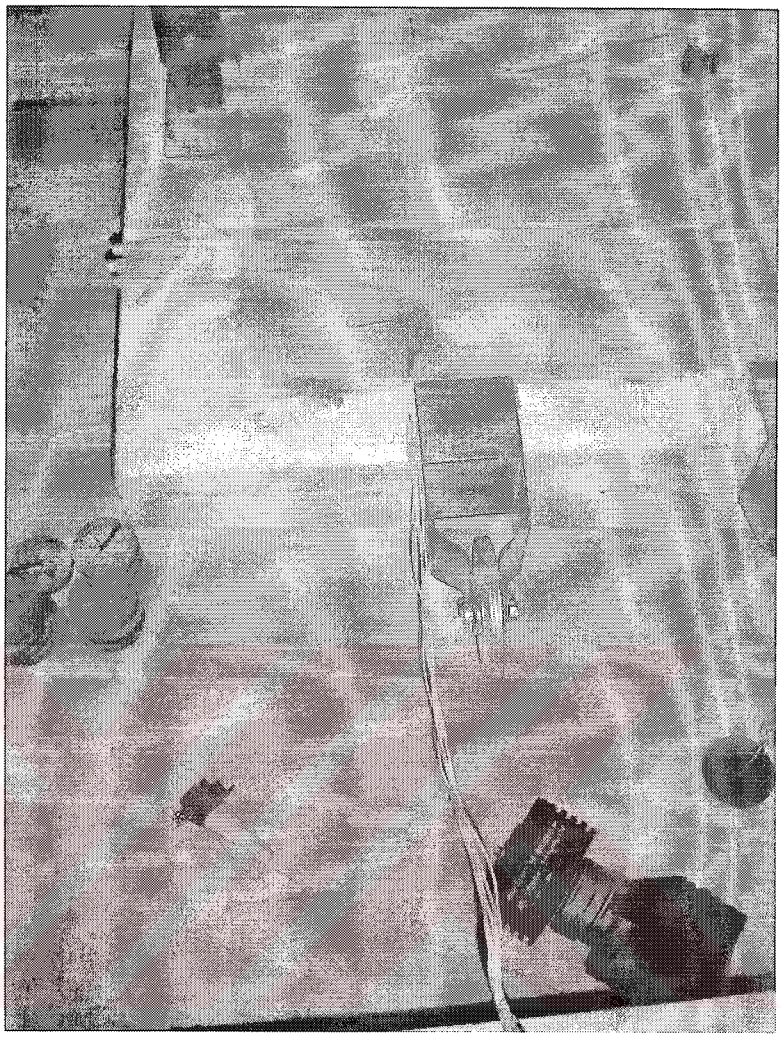

Figure 6.11 General view at the end of the Test #3

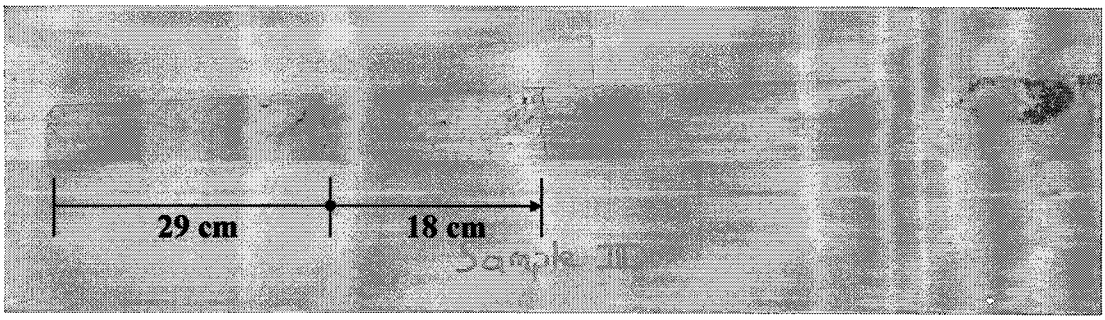

Figure 6.12 General view of the broken pile of the Test #3

6.5. Test #4: SFRC Model Pile with 0.75% ZP305&0.25(Micro) Steel Fiber

In this test a concrete pile with a fiber content of 0.75%ZP305 and 0.25%Micro, was tested. The unloading was applied when the load reached 30 and 60kg. Once the pile was completely unloaded a reloading was made until the pile was broken at 90 kg. The pile head transducers and strain-gages along the pile generated continuous data through out the test. It was observed that behavior of the pile was more rigid compared with remaining three. Pile was broken at a point 34cm below the top of the pile. The location of the breaking point on the pile was close to that of the Test #1 pile. Total pile head displacement was measured slightly different from that of the Test #1 pile being 1.40 mm. It should be mentioned that the pile was suddenly pulled out of the sand just after loaded with 100 kg. Hence, ultimate load in these tests was found as 90 kg. Although behavior of the piles in Test #1 and Test #4 are similar being more rigid than Test #2 and Test #3, the ultimate load capacity of Test #4 happened to be 1.3 times larger than the capacity of Test #1. The pile head displacement-lateral load and distribution of the moment along the pile graphs are given in Figures 6.13 and 6.14, respectively. General view of the test set-up just after the pullout of the broken pile is shown in Figure 6.15. The broken pile after the test is shown in Figure 6.16.

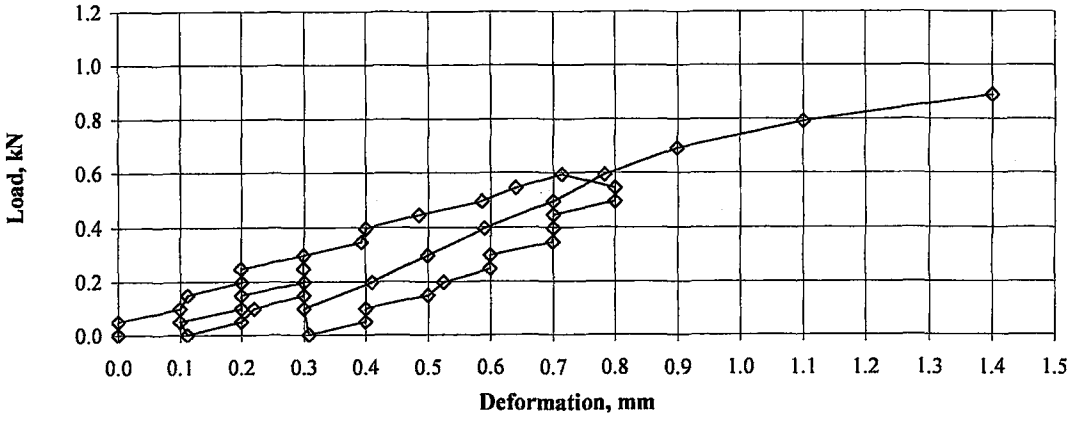

Figure 6.13 Pile head displacement for Test #4

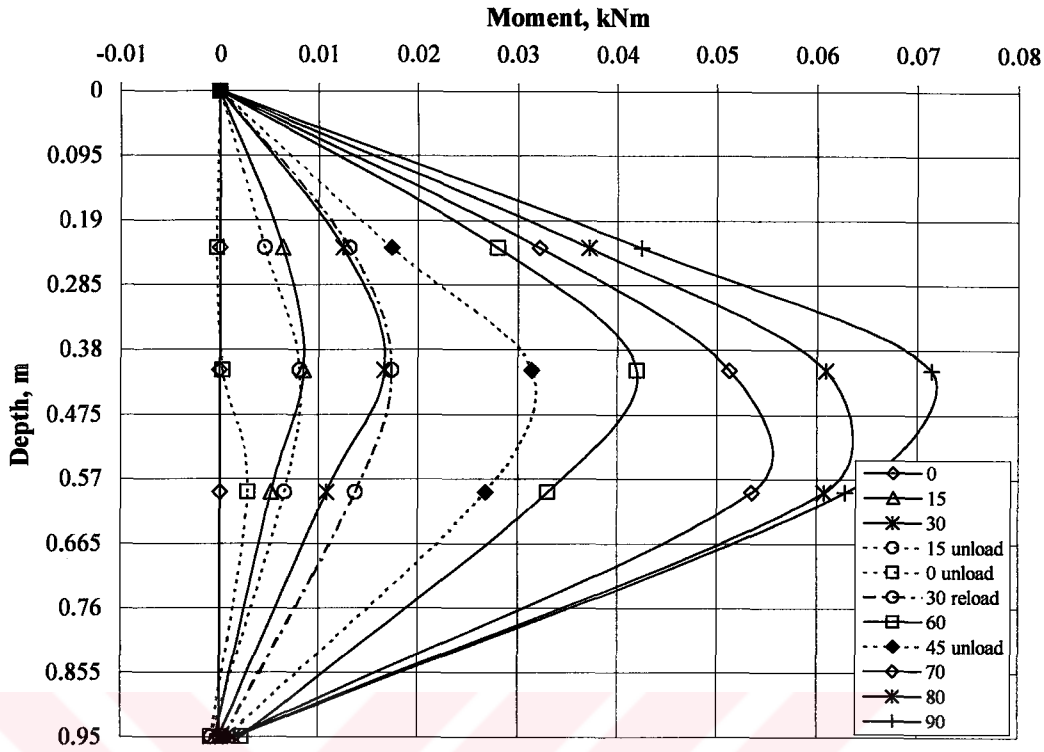

6.14 Moment distribution for Test #4

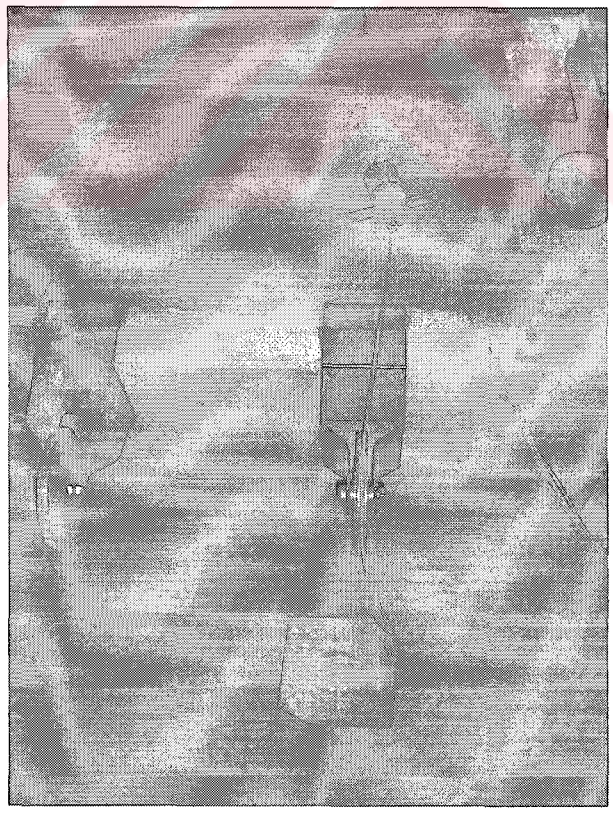

Figure 6.15 General view at the end of the Test #3

Figure 6.16 General view of the broken pile of the Test #4

6.6. Discussions

Test results may be evaluated and compared in terms of deformation and bending moment. Firstly, deformation data will be compared and discussed in the following.

Lateral load versus pile head deformation graphs of concrete and 1.5%SFRC piles may be compared in order to show pile response under lateral loading (Figure 6.17). When this figure is examined it can be seen that concrete pile exhibits higher deformations than the SFRC pile does at equal load levels. This is expected since tensile strength of conventional concrete is much lower than reinforced concrete and should also be lower than SFRC. This fact can be verified by simple strength of materials approach as in the following:

The tensile strength of the concrete produced in this study has been found as f_{ct} = 6.14 MPa. Based on this values and using Equation 6.1:

$$\varepsilon_x = \frac{1}{\rho_x} y \qquad 6.1a$$

$$\frac{1}{\rho_x} = \frac{M_x}{E \cdot I_x} \qquad 6.1b$$

$$\sigma_x = E \cdot \varepsilon_x \qquad 6.1c$$

Assuming E=3.8 x 10^7 kN/m^2 and calculating I_x=1.179 x 10^{-6} m^4, one can calculate the ultimate tensile strain as ε_x=1.616 x 10^{-4}. As mentioned above the

ultimate lateral load was somewhere between 70kg and 80kg. Corresponding bending moment at 70kg is M_x=0.07433 kNm generating a strain of $5.837x10^{-5}$. The recorded bending moment at 80kg where the broken portion of the concrete pile was suddenly pulled out of the sand 3.378 kNm resulting a tensile strain of 0.00265 which is almost one degree higher than the ultimate tensile strain. These results show that recorded pile response is in good agreement with expected concrete behavior. As can be seen in Figure 6.17 the concrete pile behaves nonlinear from the very beginning (Figure 6.18). This is an expected behavior since the concrete pile has no reinforcement at all resulting in a small crack initiation threshold.

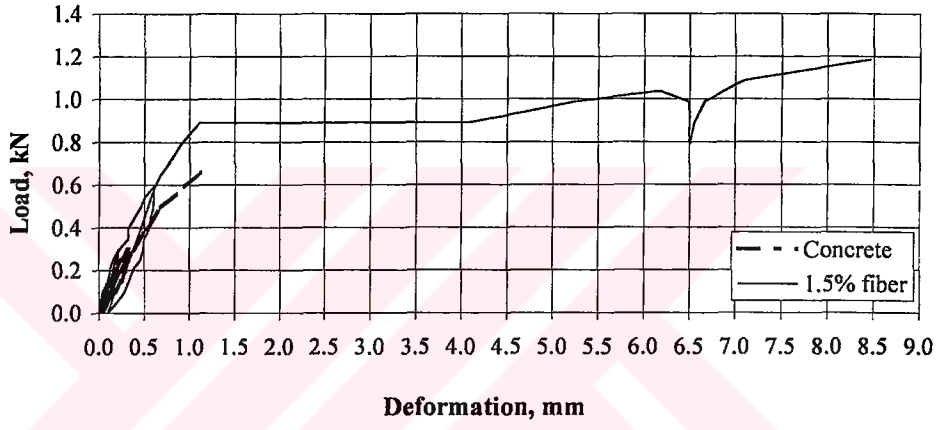

Figure 6.17 Load-deformation relationship for concrete and SFRC piles

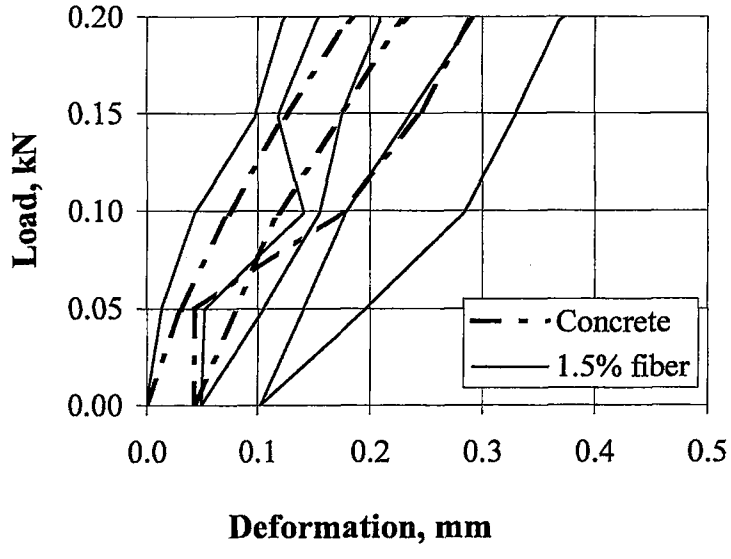

Figure 6.18 Small deformation behavior of concrete and SFRC piles

A close inspection of Figure 6.18 reveals that SFRC pile with 1.5% fiber responses more rigid than the concrete pile since steel fibers prevent early cracking of the concrete matrix. Besides ultimate lateral load for this pile was 90kg where the first plastic hinge occurred under a bending moment of 0.112 kNm. Note that lateral load and bending moment of SFRC pile are 28.6% and 50.7% higher than those for the concrete pile, respectively. This behavior is a consequence of nonlinear soil-pile interaction.

When load-deformation behavior of SFRC pile with 1.5% fiber is taken into consideration several interesting conclusions can be made. First of all SFRC pile shows smaller deformation than concrete pile under equal load as stated above. However, at any equal load level before the concrete pile breaks down the SFRC pile takes smaller bending moment (Figure 6.19).

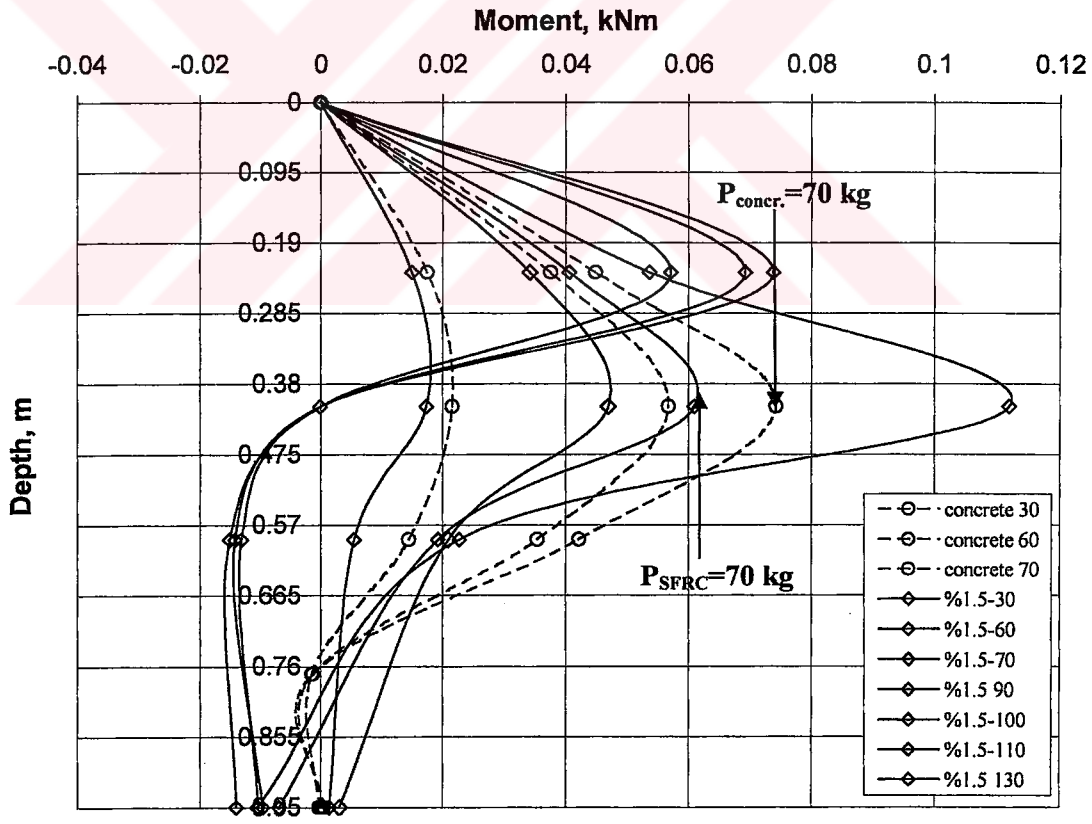

Figure 6.19 Comparison of bending moments of concrete and SFRC piles

Generation of smaller bending moments on the SFRC pile, however, is thought to be occurring due to the redistribution of moments along the more flexible SFRC pile. Since the concrete pile is stiffer than the SFRC pile, the curvature of this pile cannot stay continuous and converges to infinity resulting in higher bending moments towards failure. Overall deformation behavior of the SFRC pile on the other hand, is superior to the concrete pile until the formation of the second plastic hinge. The SFRC pile was able to carry much larger lateral loads (until 130 kg) without sudden pullout was taken place at the upper hinge.

The observed deformation shift at 90 kg, however, should be due to load transfer to the fibers from the concrete matrix. The amount of shift may depend on several factors such as the length of individual fibers, the interlocking condition of the fibers at hinge location and the distribution of the fibers in the concrete matrix. Once the fibers slip and locks again to the matrix the pile starts to take load with increasing deformation (i.e. between 4.10 and 8.5mm). The unloading branch between 6.2mm and 6.5mm (i.e. from 105 kg down to 80 kg) shows that deformations are not recoverable meaning that steel fibers do not exert any restoring force on the pile.

Following the formation of the first hinge on the pile, it is thought that the lower part of the SFRC pile below the hinge did not take bending moment. It received shear force due to the pile head load of which some portion was transferred at the hinge. The soil zone, which is in active state behind the pile, is thought to have some contribution on the response of the lower portion due to arching effect. The upper portion of the pile above the hinge starts to behave as a shorter pile until the formation of the second hinge and failure. It is noteworthy that SFRC pile can stand for higher loads as much as twice the failure load of the concrete pile.

Pictures taken at the hinge locations show that steel fibers did follow the direction of the loading indicating that they participated in pile response to lateral loading. An example is shown in Figure 6.20. The tested piles were also pictured together to demonstrate the differences and similarities between pile responses (Figure 6.21). As written in the previous sections about individual pile tests, it can be seen one more

time in Figure 6.21 that the behavior of Test #1 & Test #4 as well as Test #2 and Test #3 are similar. Plastic hinge formation is also sketched in Figure 6.22.

Figure 6.20 Steel fiber orientation with loading direction

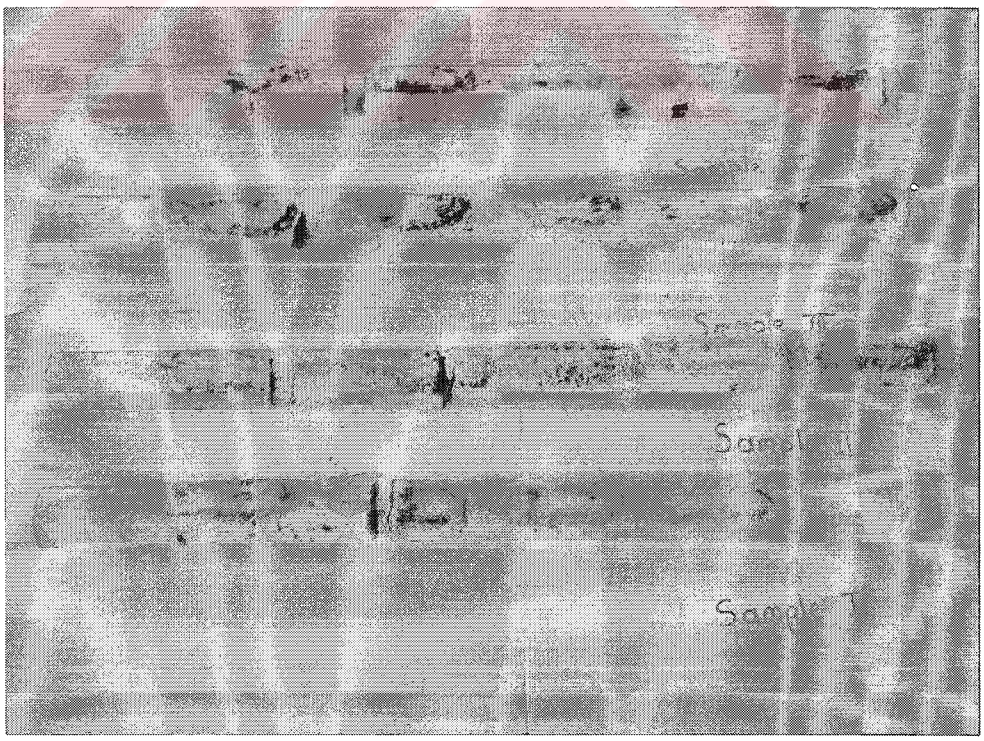

Figure 6.21 Deformed model piles following the testing study

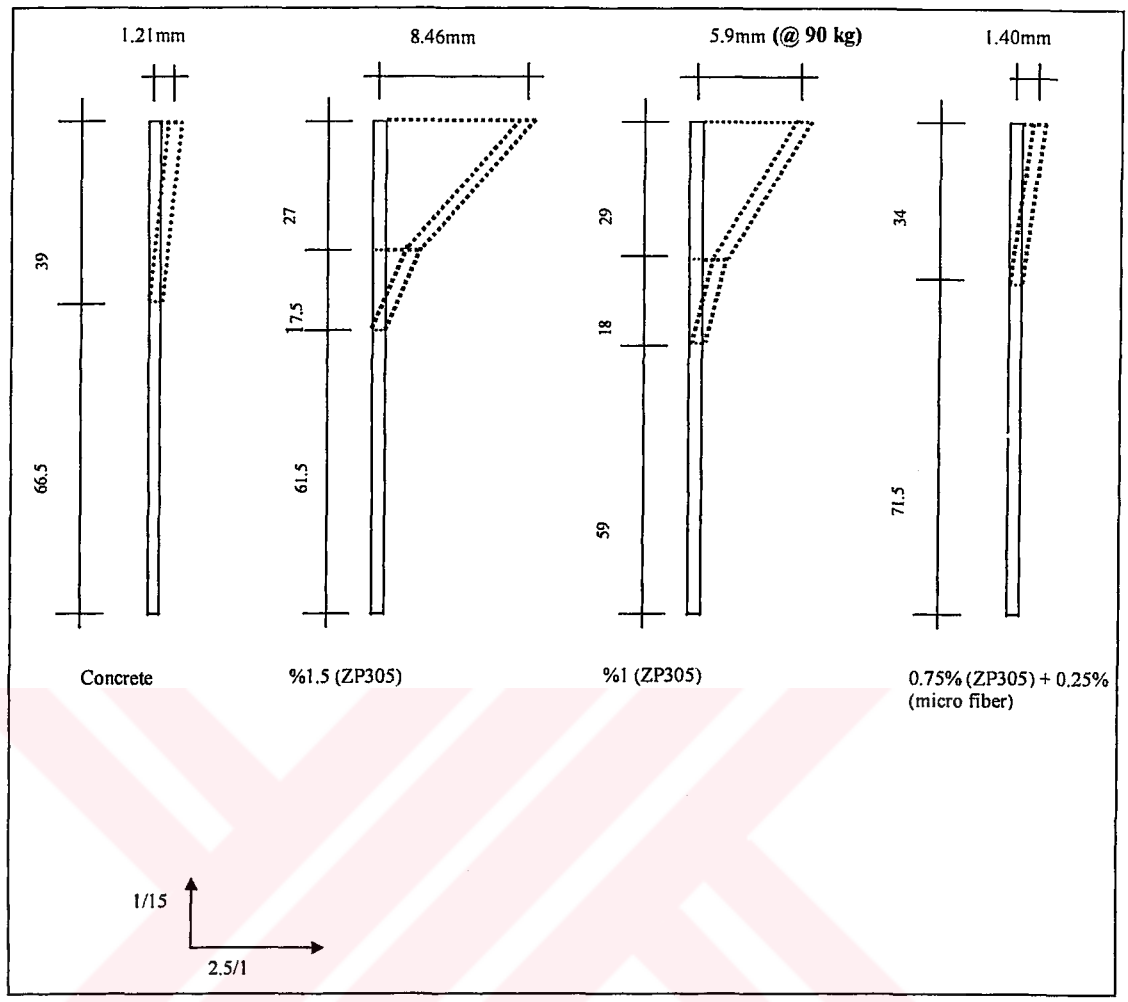

Figure 6.22 Deformation modes of model piles

It is thought that low ZP305 fiber content in Test #4 caused brittle behavior of the model pile resulting in low lateral load capacity. The tests #2 and #3, however, are very similar in nature in terms of plastic hinge formation. However, Test #3 (i.e. the pile with 1.0%SFRC) demonstrated very interesting behavior, which was not seen in any other pile: the pile stayed intact through out the test behaving as a flexible pile. One should note in Figure 6.21 that lower plastic hinge did not occur completely although the pile cracked at that point being able to transfer redistributing bending moment along the depth and transferring load to lower portion. This is shown in Figure 6.23. It can be seen in this figure that moment around the lower hinge location is lower for Test #3 showing moment redistribution. It is also notable that bending moment did not drop down to zero for Test #3.

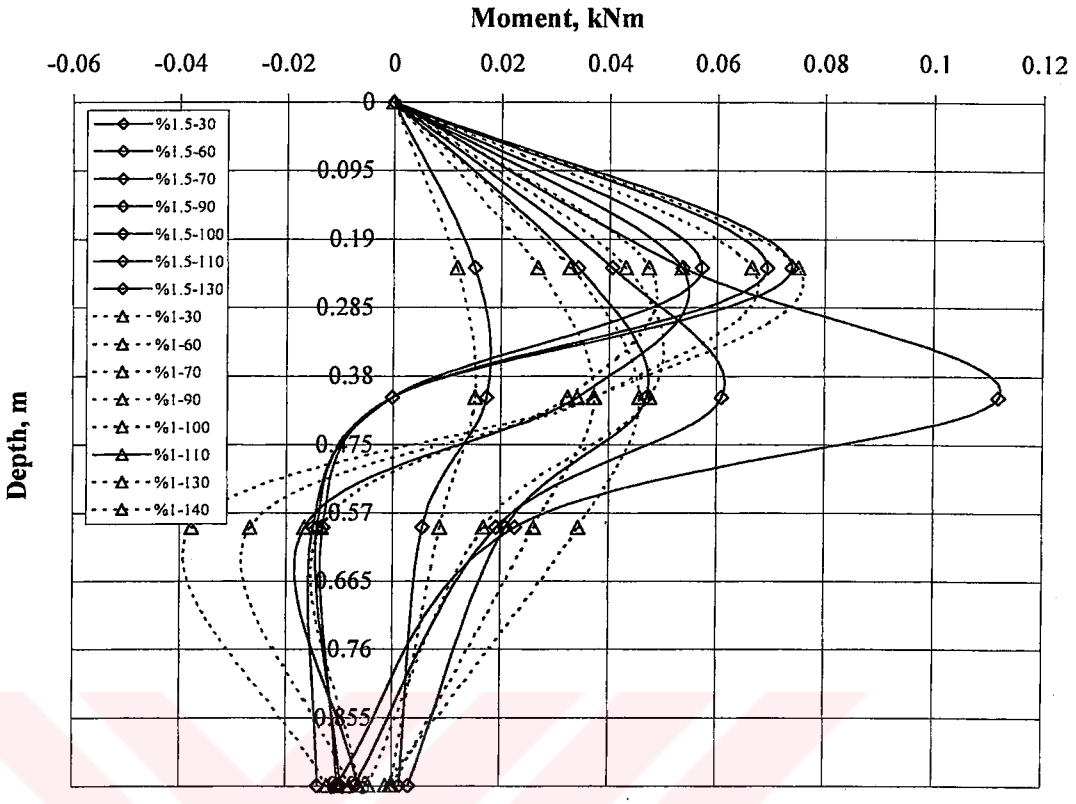

Figure 6.23 Comparison of bending moment distribution for Test #2 (1.5%SFRC) and Test #3 (1.0%SFRC)

CHAPTER SEVEN
CONCLUSIONS

Following conclusions can be made as an outcome of this thesis study:

1. Design of steel fiber reinforced concrete mix batches requires a very delicate laboratory work. It has been experienced that obeying to ACI recommendations results in production reproducible concrete batches.

2. Instrumentation and strain-gage conditioning may be troublesome in outdoor model studies. Balancing of the Whetstone bridges caused some time delays in this study.

3. SFRC piles with appropriate fiber content exhibited better performance than conventional concrete pile.

4. SFRC piles demonstrated higher energy absorbing capacity with respect to concrete pile. This fact has been observed in terms of ductile behavior of SFRC piles.

5. Lateral load carrying capacity of SFRC piles increased by a significant amount compared to the concrete pile.

6. SFRC piles showed that they could behave flexibly and redistribute bending moments at equal loads along the depth resulting in lower overall bending moment generation and higher maximum moment capacity.

7. It appears that 1.0% ZP305 would result in better pile performance. This could be due to better fiber distribution in the concrete matrix. Further study is needed in this subject.

8. Under certain amount of fiber (<1.0%) content significant improvement in pile behavior compared to concrete pile case has not been observed. Addition of micro fibers did not improve pile behavior. This observation is in agreement with the recommended fiber contents for satisfactory SFRC designs. However, more model piles may be produced with different micro fiber contents to clarify influence of this type of fiber on pile behavior.

9. Different type of fibers such as torex fiber other than hooked end type may be tried in SFRC pile production. There is a good chance of getting close to RC pile performance with such fibers.

10. It is said that axial load would significantly improve performance of SFRC structural elements as much as 400%. This would in deed be expected since axial load is expected to resist pullout mechanism of steel fibers at or near plastic hinge locations.

11. Cyclic load carrying capacity of SFRC piles is expected to be high. Large scale field test studies are needed in this subject.

REFERENCES

ACI Committee 544,(1996). State of the Art Report on Fiber Reinforced Concrete.Author.

Baguelin, F., Frank,R., Said, Y.H., (1977).Theoretical study of lateral reaction mechanism of piles.Géotechnique, 27, 405-434.

Banthia, N.,Yan,C,& Bindiganavile, (2000). Fifth RILEM Symposium on Fibre Reinforced Concretes. Rossi, P., Chanvillard, G. (Eds.), Development and Application of Hig Performance Hybrid Fiber Reinforced Concrete.

Barros, J.A.O.,& Figueiras, J.A., (1999). Flexural Behavior of SFRC: Testing and Modelling. Journal of Materials in Civil Engineering, 11, 331-339.

Bayasi, Z.,& Downey, K., (1995). Steel Fiber Reinforced Piles at Horse Mesa Dam. Concrete International, 17, 32-36

Bentur, A.,& Mindess, S, (1990). Fiber Reinforced Cementitious Composites. Elsevier Science Publishers, 41, 431-432.

Bernard, S. (2001). The Influence of Strain Rate on Performance of Fiber-Reinforced Concrete Loaded in Flexure. Cement,Concrete, and Aggregates, 23, 11-18.

Buyle-Bodin, F.,& Madhkhan, M., (2002). Performance and Modelling of Steel Fibre Reinforced Piles Under Seismic Loading. Engineering Structures, 24, 1049-1056.

Bowles, J.E., (1996). Foundation Analysis and Design.United States of America, The McGraw-Hill Companies.

Choi, O.C.,& Lee, C., (2002). Flexural Performance of Ring-Type Steel Fiber-Reinforced Concrete. Cement and Concrete Research, 33, 841-849.

Dry, C.,& Corsaw, M., (2003).A Comparison of Bending Strength Between Adhesive and Steel Reinforced Concrete with Steel Only Reinforced Concrete. Cement and Concrete Research, 33 1723-1727.

Ding, Y.,& Kusterle, W., (2000). Compressive stress-strain relationship of steel fibre-reinforced concrete at early age. Cement and Concrete Research, 30, 1573-1579

Ezeldin, A.S.,& Balaguru, P.N., 1992). Normal and high-strength fiber-reinforced concrete under compression. ASCE, 4, 415-429.

Fanella,.D.A., & Naaman, A. (1985). Stress-strain properties of fiber reinforced mortar in compression. ACI J., 82, 475-483.

Gazetas, G.,& Mylonokis, G. (1998). Geotechnical Eathquake Engineering and Soil Dynamics III. In Dakoulos, P., Yegian, M.,& Holtz, R.D. (Eds), Seismic Soil-Structure Interaction: New Evidence and Emerging Issues.

Gençoğlu, M.,& Eren, İ., (2002). An Experimental Study on the Effect of Steel Fiber Reinforced Concrete on the Behavior of the Exterior Beam-Column Joints Subjected to Reversal to Cyclic Loading. Turkish J. Eng. Env. Sci.,26 , 493-502.

Johnston, C. D., (1974). Fiber Reinforced Concrete, ACI, Steel Fibre Reinforced Mortar and Concrete-A Review of Mechanical Properties.

Koomiman, A.G., Veen, C.,& Walraven, J.C., (2000). Modelling the Post-Cracking Behavior of Steel Fiber Reinforced Concrete for Structural Design Purposes. HERON, 45, 275-306.

Kosmatka, S. H.,& Panarese, W. C.(1994). Design and Control of Concrete Mixtures. United States of America, Portland Cement Association.

Krumbach, R., Seyfarth, K., Erfurt, W.,& Friedemann, K., (1998). High Strength Concrete-Durability Investigations by Uusing the CDF-Test-First Results. LACER, 3, 57-72.

Kützing, L.,& König, G., (1999). Design Principals for Steel Fibre Reinforced Concrete-A Fracture Mechanics Approach. LACER, 4, 175-183.

Mailhot, T.,& Bissonnete, F. & Pigeon, M., (2000). Flexural Fatigue Behavior of Steel Fiber Reinforced Concrete Before and After Cracking. Materials and Structures, 34,351-359.

Mansur, M.A., Chin, M.S. & Wee, T.H., (1999). Stress-Strain Relationship of High-Strength Fiber Concrete in Compression. Journal of Materials in Civil Engineering, 11 21-29.

Mizuno, H. (1987). Pile Damage During Earthquakes in Japan (1923-1983). Response of Pile Foundations During Earthquakes.

Naaman, A.E (2003). Engineered Steel Fibers with Optimal Properties for Reinforcement of Cement Composites. Journal of Advanced Concrete Technology, 1, 241-252.

Nataraja, M.C., Dhang, N., Gupta, A. P., (1999). Stress-strain curves for steel-fiber reinforced concrete under compression. Cement& Concrete Composites, 21, 383-390.

Ozden, G., (1999). Soil-Pile Interaction in Loose Cohesionless Submerged Soils. Doctor of pholosopy dissertation. Detroit, Michigan, Wayne State University.

Romualdi, J.P& Batson, G.B. (1963). Mechanics of Crack Arrest in Concrete. ASCE, 89, 147-168.

Rossi, P., (2000). Fifth RILEM Symposium on Fibre–Reinforced Concretes. . Rossi, P., Chanvillard, G. (Eds), Ultra-High Performance Fibre Reinforced Concretes (UHPFRC): An overview.

Shah, S.P.,& Rangan,R.V.,(1971). Fiber Reinforced Concrete Properties. ACI Journal, 68, 126-135.

Simon, A., Hazar, Z., Lecointre, D.,& Petitjean,(2002) J.6th International Symposium on High,Strength / High Performance Concrete. Simon, A., Realization of two road bridges Ultra-High-Performance Fiber Reinforced Concrete.

Uğurlu, A. (1999). Çelik Liflerle Güçlendirilmiş Beton. Ankara, DSİ.